Volume 12
Number 4
April 2025
Pages 2117–2496

Environmental Science Nano

rsc.li/es-nano

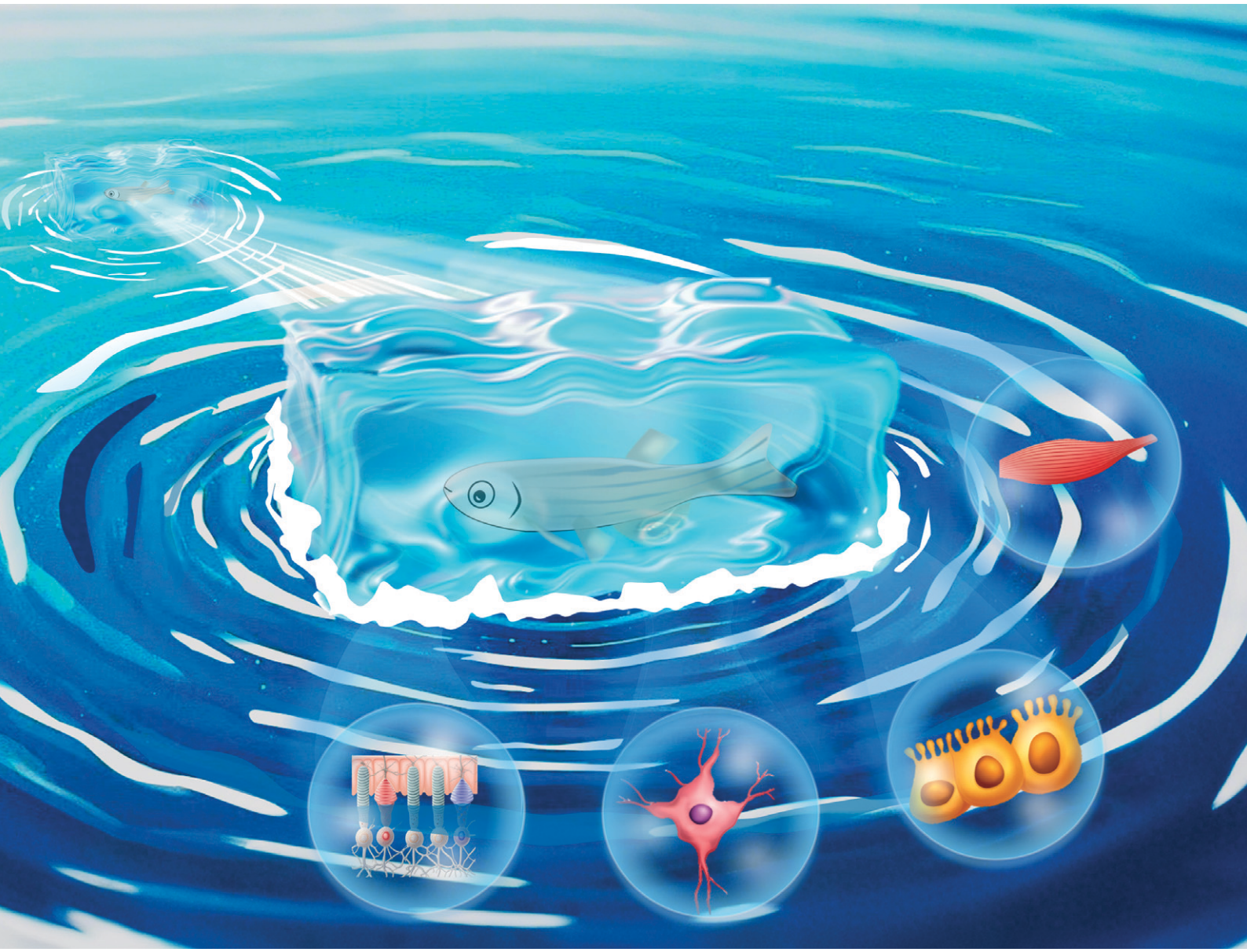

ISSN 2051-8153

ROYAL SOCIETY OF CHEMISTRY

PAPER

Mengyu Wang and Wen-Xiong Wang
Expansion microscopy revealed specific impacts of nano zinc oxide on early organ development in fish

Environmental Science Nano

ROYAL SOCIETY OF CHEMISTRY

PAPER

View Article Online
View Journal | View Issue

Cite this: *Environ. Sci.: Nano*, 2025, **12**, 2253

Expansion microscopy revealed specific impacts of nano zinc oxide on early organ development in fish†

Mengyu Wang [ab] and Wen-Xiong Wang *[ab]

Nanomaterials exhibit significant advantages in biomedical applications. However, their potential risks to organisms cannot be overlooked, particularly during early development. Nano zinc oxide (nZnO), one of the most widely used metallic nanomaterials, can have toxic effects on the early development of aquatic organisms once released into the aquatic environment. Traditional organ-specific toxicity assessment methods have limitations in exploring the nanoscale differences between materials. The novel expansion microscopy (ExM) technique allows biological samples to expand approximately 4.5-fold in three dimensions, enabling nanoscale imaging of protein and nucleic acid targets in cells and tissues using conventional optical microscopy. This study systematically assesses the toxicological changes and sources of nZnO and Zn^{2+} in the visual, skeletal muscle, and digestive systems in medaka (*Oryzias melastigma*). Our results indicated that appropriate concentrations of nZnO supported the normal early development in the visual and skeletal muscle systems, while potentially leading to excessive toxicity in the medaka digestive system. Conversely, the concentrations of nZnO suitable for the development of the digestive system may be inadequate for the needs of the visual and skeletal muscle systems. This discrepancy may arise from differences in the solubility and bioaccessibility of nZnO in gastrointestinal fluids. Further RNA sequencing revealed differences in the sensitivity of various organs in medaka to nanomaterial exposure, highlighting the necessity of implementing comprehensive risk assessment strategies in toxicology. Overall, we visualized and quantified the subtle developmental toxicities of nZnO and Zn^{2+} across different fish organs for the first time. The application of the expansion microscopy technique offered a novel perspective for evaluating the toxicity of nanomaterials.

Received 17th November 2024,
Accepted 15th January 2025

DOI: 10.1039/d4en01071j

rsc.li/es-nano

Environmental significance

Nanomaterials pose potential risks to biological systems that cannot be ignored. Nano zinc oxide (nZnO) is one of the most widely used metal nanomaterials, and once released into aquatic environments, it can exert toxic effects on the early development of aquatic organisms. Traditional organ-specific toxicity assessment methods are limited in their ability to explore the nanoscale differences between materials. The novel expansion microscopy (ExM) technique allows for the visualization of cellular and tissue protein and nucleic acid targets using conventional optical microscopy, achieving nanoscale imaging. In this study, we systematically evaluated the toxicological changes and underlying mechanisms of nZnO and Zn^{2+} in the visual, skeletal muscle, and digestive systems. Our results indicated that appropriate concentrations of nZnO supported normal early development of the visual and skeletal muscle systems but may cause excessive toxicity to the digestive system. Conversely, the concentrations of nZnO suitable for digestive system development may be insufficient for the needs of the visual and skeletal muscle systems. For the first time, we have visualized and quantified the subtle developmental toxicity of nZnO and Zn^{2+} across different organs. The application of ExM provides a novel perspective for assessing the toxicity of nanomaterials.

Introduction

With the rapid advancement of nanotechnology, nanomaterials have gained significant attention for their applications in medical translation.[1] Nanomaterials possess unique properties that offer significant potential in areas such as cancer therapy, drug/gene delivery, medical implants, and biomedical imaging.[2] While the benefits of nanomaterials are evident, their potential risks to biological

[a] *School of Energy and Environment, State Key Laboratory of Marine Pollution, City University of Hong Kong, Kowloon, Hong Kong, China.*
E-mail: wx.wang@cityu.edu.hk
[b] *Research Centre for the Oceans and Human Health, City University of Hong Kong Shenzhen Research Institute, Shenzhen 518057, China*

† Electronic supplementary information (ESI) available. See DOI: https://doi.org/10.1039/d4en01071j

systems cannot be overlooked, especially for organisms in early developmental stages.[3] The small size and unique properties of nanomaterials tend to overcome biological tissue barriers.[4] Nano zinc oxide (nZnO) severely reduces the hatching rate of zebrafish embryos and induces pericardial edema, resulting in irreversible damage to the development of various organs.[5] Gold nanoparticles can penetrate cell nuclei and bind to DNA, leading to abnormalities in early biological development.[6] Silver nanoparticles exhibit strong cytotoxicity toward male germ cells, causing developmental anomalies in subsequent generations.[7] It is therefore essential to comprehensively assess the biological toxicity effects of nanomaterials.

Currently, the techniques for studying the developmental toxicity effects of nanomaterials on biological organisms primarily focus on cytotoxicity testing, microscopy observation of tissue sections, behavioral assessments, and gene expression analysis.[8] Each of them has notable limitations. The differences between cell culture environments and *in vivo* conditions may prevent a complete reflection of the true effects of nanomaterials within biological systems.[9] The tissue sectioning process can lead to sample damage or alteration of the original structure.[10] In behavioral assessments, individual variability may severely impact the results.[11] And gene expression analysis is characterized by time sensitivity and complex data interpretation.[12] Even the emerging NanoSIMS (nano secondary ion mass spectrometry) technology faces challenges; its intricate sample preparation can affect the authenticity and comparability of the results, alongside high equipment and maintenance costs.[13] Moreover, none of these techniques provide a direct visualization of the biological toxicity caused by nanomaterials. It is noteworthy that some recently developed imaging technologies can directly visualize changes within biological organisms.[14] However, due to the resolution limitations, traditional imaging techniques have resolution limitations that hinder direct observation of organ development at the cellular level. The challenge arises from the ~200 nm optical diffraction limit of conventional optical microscopes, making it difficult to observe cellular morphology in animal samples.[15] On the other hand, electron microscopy with 2–3 orders of magnitude higher resolution provided little information about specific molecules, which were also difficult to be localized by staining.[16] Although super-resolution microscopy techniques have been developed, such as structured illumination microscopy (SIM),[17] stimulated emission depletion microscopy (STED),[18] and stochastic optical reconstruction microscopy (STORM),[19] most super-resolution microscopy technologies required specialized hardware and software. Even the most advanced super-resolution microscopy was faced with slow acquisition times, which made nanoscale imaging for large volumes of tissue samples difficult to achieve.[20] Consequently, researchers are eager to develop reliable high-resolution imaging techniques to better understand the toxic effects of nZnO on organ development.

The recently developed expansion microscopy (ExM) technique offers a reliable solution for achieving nanoscale high-resolution imaging. ExM is a cost-effective nanoscale imaging technique that allows biological samples, such as cells and tissue sections, to be isotropically expanded by ~4.5 times in three-dimensional space.[21] This enables visualization of the nanoscale organization of proteins and nucleic acids using standard microscopes.[22] Compared to conventional imaging methods, ExM overcomes the limitations of optical super-resolution techniques. Moreover, the samples after expansion with ExM contain over 98% water, making them appear transparent and thereby reducing optical aberrations.[20] From an economic perspective, the use of the ExM technique requires only a series of preprocessing protocols and a standard optical microscope, eliminating the need for complex and expensive equipment.[23] The ExM technique is continually being iteratively updated, with targeted expansion protocols developed for proteins, RNA, cells, bacteria, plants, and even small animals.[24] Currently, ExM has become a powerful imaging tool in fields such as neuroscience, clinical medicine, and nanoscience, with its accuracy and reliability widely recognized.[25]

nZnO are among the most widely used metal-containing nanomaterials, with an annual global production estimated between 550 and 33 400 tons.[26] nZnO has been widely applied in various biomedical fields, including fluorescent probes, antibacterial agents, biosensors, and drug carriers, and has garnered significant attention among numerous nanomaterials in recent years.[27] Environmental concentrations of nZnO have been documented in soil at levels ranging from 3.1–31 μg kg^{-1} and in water from 76–760 μg L^{-1}.[28] Once introduced into aquatic environments, both nZnO and the released zinc ions (Zn^{2+}) can be ingested by aquatic organisms across different trophic levels and feeding strategies, ultimately impacting public health.[29] The biological toxicity caused by nZnO and Zn^{2+} is often similar, making it difficult to distinguish between them.[30] The ExM technique effectively addresses this challenge by providing a means to visually represent and quantify the organ developmental damage at nanoscale resolution. The toxicity of nZnO is unique. Some studies identified free Zn^{2+} as the primary source of toxicity associated with nZnO,[31] while others argued that nZnO exhibited greater toxicity than dissolved Zn^{2+}.[32] Zn deficiency and Zn excess can lead to developmental toxicity in organisms.[33] Both nZnO and Zn^{2+} triggered the generation of reactive oxygen species (ROS) in organisms, leading to potential pro-inflammatory and cytotoxic effects, and exposure to 10 mg L^{-1} of nZnO completely inhibited zebrafish hatching.[34] It was reported that pericardial edema occurred as early as at 72 hpf in the 50 mg L^{-1} and 100 mg L^{-1} nZnO exposure, affecting 1.9% and 1.7% of the surviving zebrafish, respectively.[35] Additionally, nZnO is widely used as an additive in fish diets, but the implications of its dosage on nutritional deficiency and toxicity remain a matter of debate.[36] Therefore, comparing the developmental toxicity effects of nZnO and

Zn^{2+} based on different organs is essential for a comprehensive assessment of the toxicity of nZnO.

In this work, we employed an updated version of the ExM technique, capable of expanding the whole body of small animals, referred to as whole-ExM.[37] This method allowed us to conduct *in vivo* tests at the cellular level and directly visualize the damage caused by nZnO and Zn^{2+} to the early organ development in fish. We achieved nanoscale resolution imaging of the early development of representative organs including the visual system, skeletal muscle system, and digestive system of the model animal medaka in an aqueous environment. We comprehensively evaluated the differences in toxicity induced by nZnO and Zn^{2+} in the visual, skeletal muscular, and digestive systems, as well as the sources of nZnO toxicity, and found that the toxicity susceptibility to ZnO nanosensitivities varied greatly among different organs. Additionally, we combined RNA sequencing technology to compare the expression of differentially expressed genes, confirming that the toxicological differences between nZnO and Zn^{2+} are regulated by multiple genes. Overall, this study innovatively applied expansion microscopy, a technique that uniformly physically enlarges biological samples using swellable hydrogels, thereby achieving super-resolution imaging under conventional optical conditions. We have, for the first time, visualized and quantified the subtle differences in biological developmental toxicity between nZnO and Zn^{2+} in various organs. ExM can be integrated with confocal, light-sheet, and super-resolution microscopes to further enhance imaging resolution. The application of this technology enables the observation and quantification of structural changes in biological samples at the nanoscale, providing a more precise tool for the toxicity assessment of nanomaterials.

Materials and methods

Fish husbandry

Fresh medaka (*Oryzias melastigma*) eggs were sourced from the State Key Laboratory of Marine Pollution at the City University of Hong Kong. Medaka maintenance and toxicity tests followed the OECD Test Guidelines 203 and 210. The medaka eggs were incubated in 20 L water tanks with a modified simplified M7 medium (SM7 medium). The medium consisted of 0.04 mM $NaHCO_3$, 0.35 mM $CaSO_4$, 0.50 mM $MgSO_4$, 0.05 mM KNO_3, and was maintained at a pH of 7.0–7.5 for 10 d. Throughout the experiment, the water temperature was consistently maintained at 26 °C, and the photoperiod followed 14 h light/10 h dark. In this study, medaka larvae at two hpf (hours post fertilization) were collected as preparation for subsequent exposure experiments. Three replicates were instituted for each concentration treatment.

Fish diets preparation and *in vitro* dissolution test

This study mainly focuses on the toxicity effects of nZnO exposure in aquatic environments, thus we prepared nZnO-diets. We investigated the Zn content of common commercial diets (Fig. S1†), which ranged from 70.8 ± 3.3 to 149.0 ± 3.6 μg g^{-1}. The commercial diets on the market were inherently high in Zn. To ensure that our final diet additions were accurate, we first configured a Zn-free basal diets on which to add Zn. Using this method, we can accurately weigh and add Zn, and make sure that Zn was added in the form of Zn ions or Zn oxide nanoparticles to compare the toxic effects of different concentrations as well as different forms of Zn in terms of control variables. First, we prepared the formulation of Zn-free basal diets based on the nutritional requirements of fish for the subsequent addition of nZnO, the specifications are shown in Table S1.†[38] We then introduced liquid forms of Zn^{2+} and nZnO (spherical, 10 nm, Brofos Nanotechnology (Ning Bo) China) into the Zn-free basal diets powder. The size distribution of nZnO was characterized by a scanning electron microscope. The Zn content of nZnO was selected based on the nutritional requirements of fish and the Zn content of commercially available diets. The selection of 70 μg g^{-1} Zn was established from an earlier study, which represented the normal developmental supplementation level for medaka.[39] The nZnO (70 μg Zn per g diet) served as a relatively low-level nZnO treatment and the Zn^{2+} (70 μg Zn per g diet) served as the control group to ensure the same Zn exposure dose as the treatment, and previous studies have shown that this level can meet the early development needs of medaka.[39] nZnO (150 μg Zn per g diet) and Zn^{2+} (150 μg Zn per g diet), which were also commercially available, served as high-level Zn treatments to investigate the differences in the toxicity effects of nZnO and Zn^{2+} on organ development. Overall, we set up the following four treatment groups: nZnO (70 μg Zn per g diet) (low-level nZnO), nZnO (150 μg Zn per g diet) (high-level nZnO), Zn^{2+} (70 μg Zn per g diet) (control group), and Zn^{2+} (150 μg Zn per g diet) (high-level Zn^{2+}). Zn content in all diets on a dry weight basis. For the administration of the dosage of μg g^{-1} (70 μg g^{-1} was used as an example), we first dissolved 35 mg of Zn (corresponding quality of $ZnCl_2$ and nZnO) in sufficient deionized water and mixed the Zn solution homogeneously. The amount of deionized water was ensured to completely immerse 500 g of the Zn-free basal diets powder. We then poured this Zn solution into 500 g of Zn-free basal diets powder to produce a slurry and mixed it thoroughly and homogeneously multiple times. The mixture was freeze-dried, thoroughly pulverized, and homogenized into a powder to facilitate consumption by the medaka. During the whole diet preparation process, we controlled the conditions to avoid the dissolution of Zn from nZnO as much as possible. Specifically, the feed powder in the wet state was minimized to avoid possible dissolution. To investigate the state of dissolved Zn^{2+} in SM7 medium, we used Visual MINTEQ software to calculate concentrations and activities of aqueous inorganic species after Zn^{2+} (70 μg Zn per g diet), Zn^{2+} (150 μg Zn per g diet), nZnO (70 μg Zn per g diet), and nZnO (150 μg Zn per g diet) dissolution in the SM7 medium at pH 7.0 for 30 min, as shown in Tables S2–S5.† The results showed that the concentration of Zn^{2+} in

the SM7 medium was significantly higher than the complexed state formed with other inorganic salt ions. Therefore, we considered Zn^{2+} to exist in the free state and ignored the other complex states. Then, each diet underwent acidification, digestion, and subsequent determination of actual Zn content utilizing ICP-MS (NexION 300X, PerkinElmer, USA). To assess the Zn^{2+} dissolution rate from diets, the modified diets were dissolved in an SM7 medium with gentle shaking, and the Zn concentration in the solution was measured after 1 h.

When exploring the toxicity of nZnO, its dissolved Zn^{2+} cannot be ignored. To simulate the *in vivo* dissolution rate of Zn^{2+} from nZnO, we performed *in vitro* simulated gastrointestinal fluid testing. Medaka digestive fluids were modified based on the commonly used *in vitro* digestion methods.[40] The composition of the simulated gastrointestinal fluid and the digestion time setting in this method were referenced from the physiological digestive characteristics of the model organism zebrafish, and were also applicable to medaka. The materials included simulated gastric control fluid (SGFc, pH 2.0, 2 mg mL^{-1} NaCl), gastric fluid (SGF, 4 mg mL^{-1} pepsin in SGFc), intestinal control solution (SIFc, pH 6.8, containing 6.8 mg mL^{-1} KH_2PO_4 and 0.616 mg mL^{-1} NaOH), intestinal fluid (SIF, 10 mg mL^{-1} pancreatin in SIFc), and bile solution (SBS, containing 4 mM sodium taurocholate and 4 mM sodium glycodeoxycholate in SIFc), all prepared in Milli-Q water. For the digestion tests under simulated gastric conditions in medaka, the diets were incubated in 6.25 mL of SGFc at 37 °C for 10 minutes. Following the addition of 1.25 mL of SGF and pH adjustment to 2.0 ± 0.1 using a 1 M HCl solution, the mixture was shaken in a thermostat oscillator at 167 rpm and 37 °C for 10 min. Subsequently, the solution was statically incubated at 37 °C for 2 h. The digestion was then transitioned to the intestinal phase by adjusting the pH to 6.8 and increasing the total volume to 8.75 mL using SIFc. After adding 0.25 mL of bile solution and 1 mL of preheated SIF (to 37 °C), the mixture was shaken at 170 rpm and 37 °C, and 2 mL of supernatant was collected after 4 h. All collected samples were centrifuged at 12000 rpm for 10 min to remove debris to determine the dissolved Zn^{2+}. Each treatment was replicated three times.

Zn bioaccumulation in fish

Newly hatched medaka larvae were collected and exposed to the modified diets. Fifty larvae per container were placed in a 1 L container filled with SM7 medium, maintained at a water temperature of 25 °C. Medaka were fed with the modified diets at 9 am, 2 pm, and 9 pm daily. The quantity of diets provided was carefully tested and controlled to confirm that the medaka was able to completely consume the dietary powder. In instances where trace amounts of the dietary powder remained unconsumed, they were meticulously collected, freeze-dried, and then weighed using a high-precision instrument. The mass of the uneaten diet was subsequently subtracted from the final calculations to enhance the accuracy of the dietary intake measurements. Following a 30 min feeding period, the medium was replaced with a clean SM7 medium. We weighed the total mass of diets before and after exposure, and the difference was used to calculate the daily diet consumption rate (*i.e.*, 0.08 mg per fish). After 3, 8, and 14 d of dietary exposure, medaka was collected and anesthetized with tricaine (0.01% ethyl 3-aminobenzoate methanesulfonate salt, Sigma-Aldrich). Under the dissecting microscope, samples were fixed using a precision surgical blade, while a sharp pair of forceps was employed to separate the eyes from the body. The isolated eyes and bodies were individually weighed using a precision balance and preserved in 1 ml centrifuge tubes. These specimens were designated for subsequent Zn accumulation quantification and expansive microscopy imaging. The samples were placed in 100 μl of 65% HNO_3 and digested at 80 °C overnight, the Zn concentration was then determined by ICP-MS.

Expansion microscopy imaging in fish

In the study of nZnO's toxic effects on organ development, nanoscale visualization and quantification of changes are essential. Although electron microscopy offers high resolution, it lacks molecular specificity and cannot image live samples.[16] Super-resolution techniques such as SIM, STED, and STORM provide a middle ground, enhancing resolution beyond conventional microscopy while permitting live-sample imaging and specific molecule localization.[17–19] Nonetheless, these methods face challenges due to slow acquisition times and the requirement for specialized equipment. Thus, developing new high-resolution imaging techniques to surmount these obstacles is crucial for deepening our understanding of the toxicological impacts of nZnO and other nanomaterials. This study utilized expansion microscopy (ExM) to attain nanoscale imaging of diverse medaka organs. ExM was not an optical microscope but rather a novel imaging technique.[41] This method enabled the sample to expand uniformly through a series of chemical means, which can effectively improve the resolution of imaging under a common confocal microscope.[41] The principle of expansion has been widely used in fields such as biological and medical imaging.[42] The procedure mainly included fixation, anchoring, gelation, digestion, staining, decalcification, and expansion.[37] The protocol of the ExM was described in the supplementary note. After the last step expansion, gel samples were placed on a 24 mm × 60 mm microscope glass and imaged on the Zeiss LSM 900 confocal microscope using two different channels for gel imaging. Channel 1: excitation/emission 488/495–525 nm; channel 2 excitation/emission 647/655–685 nm. A 40× 1.3 NA oil immersion lens and a 20× 0.45 NA air lens were employed.

Transcriptomic analysis of fish in response to dietary nZnO and Zn^{2+}

RNA sequencing was employed to elucidate the intricate molecular responses in medaka subjected to dietary nZnO and Zn^{2+}. Following a 14 d exposure to varying dietary levels, the whole body of the medaka sample was collected, preserved in liquid nitrogen, and stored at −80 °C. Subsequent total RNA extraction from medaka utilized TRIzol® reagent, followed by transcriptome sequencing conducted by Biomarker Technologies, Beijing, China. The resequencing raw data of medaka (*Oryzias melastigma*, wild type) in this study have been uploaded to the NCBI Sequence Reading Archive (SRA) with accession number PRJNA1141718. Data analysis was performed using BMKCloud. The analysis of differential gene expression employed DESeq2, with gene expression differences ($p < 0.05$) considered as statistically significant differential expression.

Quality assurance/quality control and statistical analysis

In this study, data were presented in terms of means and standard deviations. The quantification of Zn concentrations in the medaka was documented based on a dry weight (dw). Throughout the Zn analyses conducted by ICP-MS, each treatment involved three replicates, with the inclusion of standard fish tissue reference material (IAEA-467, International Atomic Energy Agency Reference Materials Group) for stringent quality control. The confocal images of different organs were processed using ZEN 3.5 (blue version) and Fiji software. Comprehensive data analyses were executed by SPSS (version 25.0) for one-way analysis of variance (ANOVA) with Bonferroni correction. The graphical representations in figures were generated through Origin 2018. The significance threshold was established at 5%.

Ethical statement

All animal procedures were performed in accordance with the Guidelines for the Care and Use of Laboratory Animals of City University of Hong Kong University and approved by the Animal Ethics Committee of City University of Hong Kong.

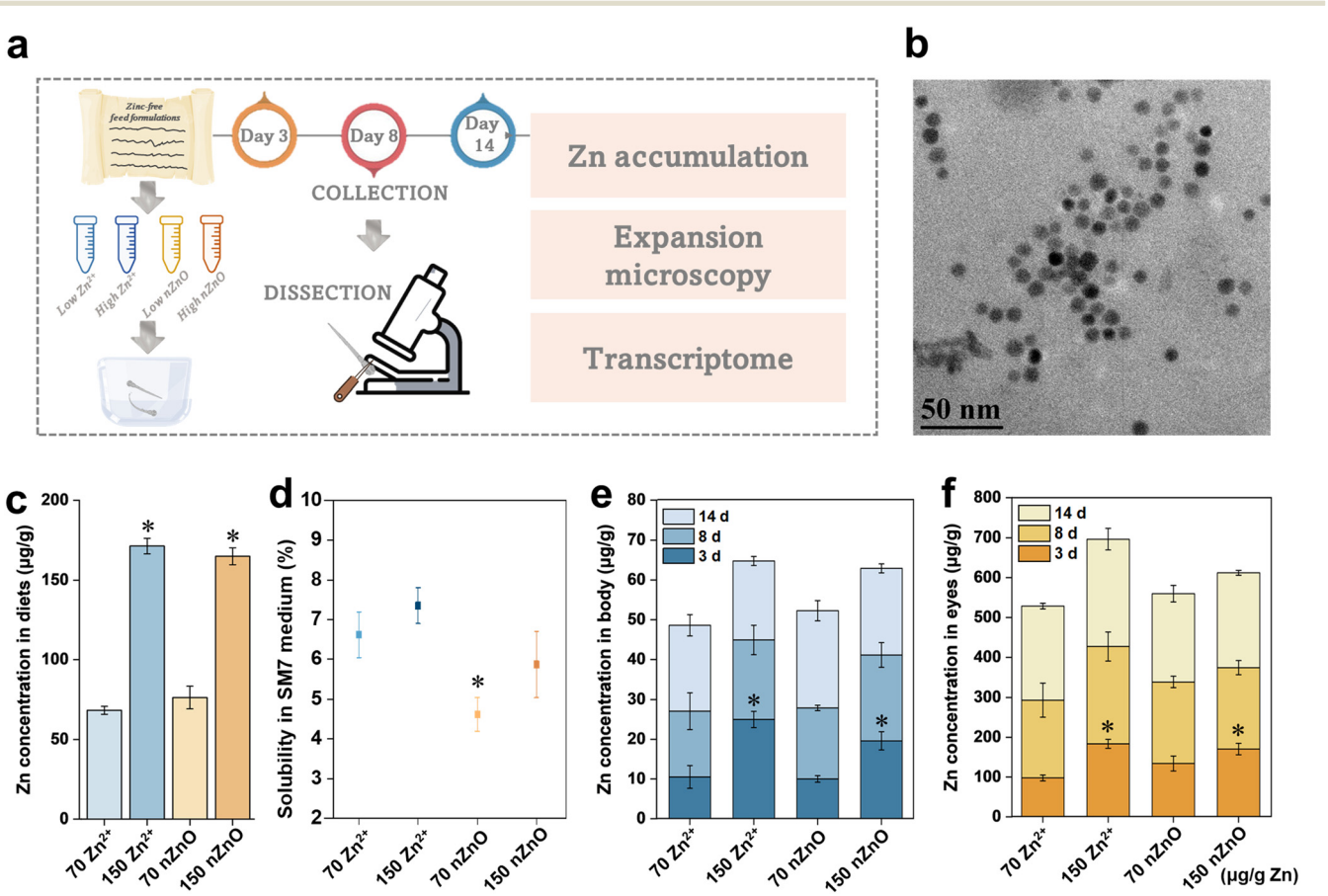

Fig. 1 Zn contents in the modified diets and Zn accumulation in fish. (a) Diagram of experimental design. This included preparation of the modified diets, dietary exposure, collection, dissection, and subsequent analysis. (b) SEM image of nZnO. (c) Zn contents in modified diets. (d) The dissolution rate of different kinds of diets in SM7 medium. (e) Zn accumulation in fish body parts other than the eyes after modified diets Zn exposure. (f) Zn accumulation in fish eyes after modified diets Zn exposure. Data are expressed as mean ± SD (n = 5). *$p < 0.05$, compared with the control (Zn^{2+} (70 μg Zn per g diet)). The numbers 70 and 150 on the graph are the Zn content in μg g^{-1}.

Results and discussion

Zn contents in modified diets and fish

Medaka larvae were fed with nZnO and Zn^{2+} modified diets for a continuous period of 14 d and collected the larvae on the third, eighth, and fourteenth days. We then separated the eyes and body for subsequent measurements (Fig. 1a). The SEM image of nZnO is shown in Fig. 1b, which was characterized by uniform particle size. The actual Zn contents of the prepared diets were 76.4 ± 7.1 μg g^{-1} for the nZnO (70 μg Zn per g diet), 68.4 ± 2.6 μg g^{-1} for the Zn^{2+} (70 μg Zn per g diet), 165.0 ± 5.3 μg g^{-1} for the nZnO (150 μg Zn per g diet), and 171.4 ± 4.9 μg g^{-1} for the Zn^{2+} (150 μg Zn per g diet), which were consistent with the exposure concentrations of the experimental design (Fig. 1c). The feeding duration for medaka was 30 min each time. The diets dissolved in SM7 medium after 1 h represented the maximum dissolution rate of the diets in SM7 medium. Dissolution rates in SM7 medium of all diet types in SM7 were less than 8% (Fig. 1d), suggesting that nZnO diets and Zn^{2+} diets had limited dissolution rate in the SM7 medium. We thus assumed that Zn was exposed to the fish in the form of nZnO and Zn^{2+}. We then measured the Zn accumulation in the eyes and body parts (excluding the eyes) of medaka on days 3, 8, and 14 of exposure. The reason for measuring the eyes separately was that eye development required extraordinarily high Zn levels during early development.[43] Satisfying the Zn developmental needs of the eyes meant that the overall Zn levels were adequate.[39] For each diet, Zn accumulation in the eyes increased during the 3–14-day exposure. Zn accumulation in body parts was different, with the Zn^{2+} (70 μg Zn per g diet) and nZnO (70 μg Zn per g diet) groups showing an increasing trend during 3–14 days of exposure, whereas nZnO (150 μg Zn per g diet) did not show significant change from 3–14 days, and the Zn^{2+} (150 μg Zn per g diet) group showed a decreasing trend from 3–8 days (Fig. 1e and f). Compared to the control group, the Zn^{2+} (150 μg Zn per g diet) and nZnO (150 μg Zn per g diet) in the eyes and body parts showed a significant increase in Zn accumulation on day 3, whereas the subsequent exposure showed no significant change during the corresponding period (Fig. 1e and f). This may be related to the mRNA expression of Zn transporters, among which ZnT1, ZnT5, ZIP3, and ZIP10 were expressed differently due to changes in Zn status. Earlier studies showed that the mRNA level of Zn exporter ZnT1 in zebrafish treated with excess Zn was upregulated, but was downregulated under Zn deficiency.[24,44] During the later stages of exposure, Zn regulation may also result in no significant change in Zn body accumulation.

Dissolution of the formulated Zn^{2+} diets and nZnO diets in SM7 medium was then quantified. The actual release of Zn from the diets was only 4.34, 11.03, 3.78, and 9.57 μg L^{-1} for the Zn^{2+} (70 μg Zn per g diet), Zn^{2+} (150 μg Zn per g diet), nZnO (70 μg Zn per g diet), and nZnO (150 μg Zn per g diet), respectively (Fig. 1d). We simulated their dissolution during fish feeding by measuring the diet solubility after 1 h in SM7 medium. The Zn solubility of amended diets was less than 8% and the actual feeding time was less than the simulated dissolution time, thus the amount of Zn^{2+} dissolved in the medium was limited. It was therefore presumed that the toxicity originated from Zn^{2+} released from nZnO in the body rather than Zn^{2+} dissolved in the SM7 mediums. In previous studies, exposure to waterborne Zn up to 200 μg L^{-1} showed an accumulation of ~162 μg g^{-1} Zn in the eye after 12 days of exposure, which was significantly lower than the value in this study.[39] Thus, dietary exposure probably contributed to the accumulation of Zn in the eyes through ingestion, digestion, and absorption.[45,46] Furthermore, Zn accumulation in the eye was nearly 10 times higher than in the body, presumably due to its high Zn demand during early developmental stages.[47] It was reported that the average Zn concentration in the retina was as high as 296 μg g^{-1}, 488 μg g^{-1}, and 1069 μg g^{-1} in the salmon, squirrelfish, and red snapper, respectively, as compared to the typical concentration of around 20 μg g^{-1} in fish muscle.[48]

Variations in developmental patterns of visual system in fish

Previous studies of organ development focused on traditional methods such as *in vivo* imaging, immunostaining of fixed tissues, and *in situ* hybridization, which are unable to observe and quantify subtle developmental changes in cellular structures due to resolution issues.[47] The expansion microscopy successfully imaged the microscopic structure of fish organs with nanoscale resolution. Before imaging, the dimensions of each gel sample were measured before and after expansion to ensure uniform expansion at a ratio of 3.9 ± 0.1 times length. The hydrophobic fluorophore ATTO 647 N NHS ester provided vibrant staining of lipid-rich structures, specifically the nuclear membranes, thereby elucidating intricate organelle structures and aiding in the distinction of diverse cell types (Fig. 2, magenta). In contrast, the hydrophilic fluorophore Alexa Fluor 488 NHS ester highlighted the nucleoplasm and cytoplasm, thus delineating the comprehensive morphology of cells (Fig. 2, green). The pH of the ExM buffer solution was pivotal for preserving the structural integrity of hydrogels and biological specimens. An optimal pH of approximately 7.4 was essential for hydrogel stability and the maintenance of biological architecture.[49] Variances from this pH can precipitate hydrogel degradation and specimen distortion. Temperature is another critical factor in the expansion process; it should be conducted at ambient temperatures ranging from 20–25 °C to circumvent thermally induced degradation of hydrogels and biological samples. Elevated temperatures may expedite hydrogel degradation, whereas reduced temperatures can impede the expansion process.[50] Our study strictly controlled the influence of environmental factors, including pH and temperature, to improve the reliability of our research results. Furthermore, ExM has been effectively utilized across diverse species, including mouse embryos and zebrafish, as evidenced by the successful application in neuroscience and

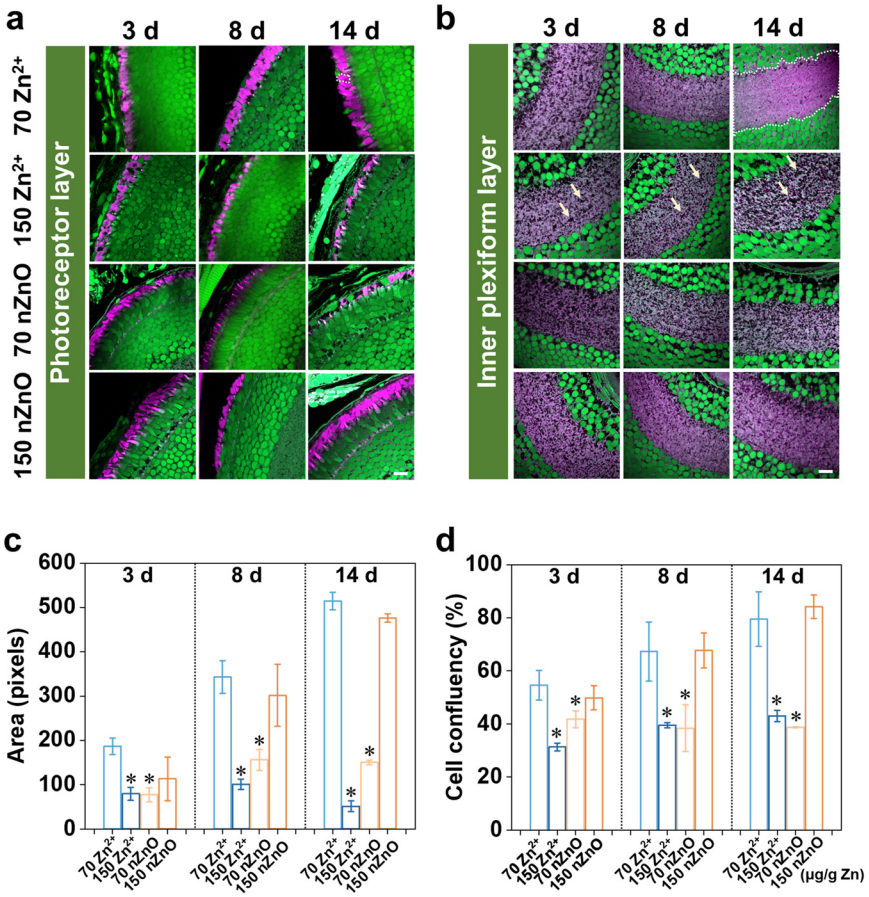

Fig. 2 Variation in expansion microscopy imaging and cellular quantification of medaka retinal parts due to different Zn exposure. (a) Expansion microscopy imaging of photoreceptor cells of medaka exposed to nZnO diets and Zn^{2+} diets during 14 d continuous exposure. (b) Expansion microscopy imaging of inner plexiform cells of medaka exposed to nZnO diets and Zn^{2+} diets during 14 d continuous exposure. (c) Quantification of variation in photoreceptor cell area in medaka exposed to nZnO diets and Zn^{2+} diets. (d) Quantification of variation in inner plexiform cell area in medaka exposed to nZnO diets and Zn^{2+} diets. Green, Alexa Fluor 488 NHS ester; magenta, ATTO 647 N NHS ester. Data were expressed as mean ± SD (n = 10). *$p < 0.05$, compared with the control (Zn^{2+} (70 μg Zn per g diet)). Scale bars: 10 μm. All length scales are presented in pre-expansion dimensions. The numbers 70 and 150 on the graph are the Zn content in μg g^{-1}.

developmental biology studies.[22] Based on the above, we investigated the impact of nZnO and Zn^{2+} on the developmental patterns of retinal cells, skeletal muscle cells, and intestinal epithelial cells employing different Zn exposure patterns to investigate the variation in the effects brought about by nZnO and Zn^{2+} on different organs.

Eye development is highly sensitive to Zn during early developmental stages.[51] Polluted discharges of nZnO and artificially fed diets may impact the early development of the visual system in aquatic organisms. The area and arrangement of the photoreceptor layer cells of the fish retina can be used as one indicator to assess their developmental status. Normally developed photoreceptor cells usually have a more uniform size and tightly ordered arrangement, while abnormally developed or affected cells may show features such as uneven size and disorganized arrangement.[52] In this study, as shown in Fig. 2a, in the Zn^{2+} (70 μg Zn per g diet) group (as the control group), the photoreceptor cells showed a dense arrangement with an increase in the number and area of the cells during 14 d development, which was positively able to meet the Zn exposure for retinal development. In the nZnO (70 μg Zn per g diet) group, after 3 d exposure, the arrangement of photoreceptor cells showed a tendency to be skewed. On day 8 and day 14 with the increase of exposure time, their number and area decreased, especially on day 14, the photoreceptor cells appeared to be defective and deformed (Fig. 2a). The cell area of Zn^{2+} (70 μg Zn per g diet) treatment increased, while the photoreceptor cell area of nZnO (70 μg Zn per g diet) treatment did not change significantly and was significantly lower than that of Zn^{2+} (70 μg Zn per g diet) group on day 3, 8 and 14, respectively (Fig. 2c). In the nZnO (150 μg Zn per g diet) treatment, although cell development was slower, cell arrangement remained relatively dense (Fig. 2a). Quantitative results of cell area indicated that compared to the control group, cell development in the nZnO (150 μg Zn per g diet) treatment appeared relatively normal, with cell area increasing with exposure time (Fig. 2a and c). Compared with Zn^{2+}, nZnO (70 μg Zn per g diet) caused nutrient deficiencies in photoreceptor cells, leading to developmental toxicity,

whereas high concentrations of nZnO released more Zn^{2+} to satisfy the developmental requirements. Notably, photoreceptor cells treated with Zn^{2+} (150 μg Zn per g diet) showed severe defects, and the cellular arrangement was distorted on day 14 of exposure (Fig. 2a). Quantitative results showed a significant reduction in the cellular area during development (Fig. 2c). Thus, the Zn^{2+} (150 μg Zn per g diet) provided excessively high levels of Zn, leading to developmental toxicity in photoreceptor cells, compared to the controls that maintained normal development.

The inner plexiform layer was one of the important structures in the retina responsible for transmitting neural signals, and its development directly affected the function and performance of the visual system.[53] It can also be used as one indicator to assess the developmental status. Usually, a normally developed inner plexiform layer exhibits a tightly organized arrangement and high cell density, which facilitates the transmission and processing of neural signals, thus safeguarding the normal operation of visual functions.[53] On the contrary, an abnormally developed or disturbed inner plexiform layer may exhibit features such as irregular arrangement and sparse cellularity, resulting in abnormal or blocked neural signaling.[53] In this study, for the inner plexiform layer, imaging showed that the inner plexiform layer treated with Zn^{2+} (70 μg Zn per g diet) was densely developed and the group treated with nZnO (70 μg Zn per g diet) was sparsely porous (Fig. 2b). From the quantitative results, it can also be seen that with increasing exposure time, the cell densities of the Zn^{2+} (70 μg Zn per g diet) treated increased, while the cell densities of the nZnO (70 μg Zn per g diet) treatment had no significant change (Fig. 2d). On days 3, 8, and 14, the cell density of inner plexiform layer cells in the nZnO diets group was significantly lower than that in the Zn^{2+} diets group, which suggested that nZnO (70 μg Zn per g diet) was toxic to the inner reticular layer cell development compared to Zn^{2+}, resulting in impaired cell development (Fig. 2d). However, there was no significant change in cell density in the nZnO (150 μg Zn per g diet) exposure group relative to the control group (Fig. 2d). This indicated that compared with Zn^{2+}, nZnO (70 μg Zn per g diet) caused nutrient deficiencies in inner plexiform layer cells, leading to developmental malformation, whereas high levels of nZnO can prevent this malformation. In addition, the cell development of the Zn^{2+} (150 μg Zn per g diet) group demonstrated cellular thinning, with visible pores (at the arrows) from day 3 and significantly reduced cellular confluency, suggesting a toxic effect of Zn^{2+} (150 μg Zn per g diet) on the development of inner plexiform layer as well. Overall, compared to the control group, nZnO (70 μg Zn per g diet) failed to meet the developmental needs of the two retinal cells and caused developmental damage from Zn deficiency. nZnO (150 μg Zn per g diet) was not significantly different from the control and met the early developmental Zn needs of both cell types, whereas the Zn^{2+} (150 μg Zn per g diet) provided excessively high Zn levels and caused toxicity to retinal cell development. The total Zn content of the ionic Zn and nZnO with the same Zn level was constant, thus the developmental effects should be due to differences in Zn form.

Variations in developmental patterns of skeleton muscle system in fish

In this study, we mainly focused on the skeletal muscle and spinal cord which were closely linked to skeletal development and had an important influence on fish survival and reproductive behavior.[54] The skeletal muscle accounts for 40–60% of the fish's weight and is the largest tissue in the fish body, which plays a crucial role in the growth of the fish trunk.[55] The basic structure of skeletal muscle is the muscle fiber, and the formation of skeletal muscle is essentially an increase in the number of muscle fibers (hyperplasia) and the volume of muscle fibers (hypertrophy).[56] Their main functions are to generate movement, maintain body posture and position, maintain body temperature, store nutrients, and stabilize joints.[57] The skeletal muscles attached to the spine are involved in casual movements and promote locomotion and posture.[58] Therefore, we imaged skeletal muscle and spinal cord region by the whole-ExM method and then quantified the area of the skeletal muscle cells and density of spinal cord cells to investigate the variation in the effects of nZnO and Zn^{2+} on the skeleton muscle system.

In skeletal muscle, the muscle fibers of medaka exposed to the Zn^{2+} (70 μg Zn per g diet) were tightly packed, with an increase in muscle cell area and a decrease in cell gaps with increasing exposure time (Fig. 3a). In contrast, the muscle fibers of medaka exposed to the nZnO (70 μg Zn per g diet) were loosely aligned by the third day, and the gaps between skeletal muscle cells increased with exposure time (Fig. 3a). From the cellular quantification results, the Zn^{2+} (70 μg Zn per g diet) resulted in an increasing trend in the skeletal muscle cell area, indicating that skeletal muscle was able to develop during exposure. The cell area treated with the nZnO (70 μg Zn per g diet) was significantly lower than that of the Zn^{2+} diets exposed cells on both 8 d and 14 d, indicating that relative to the Zn^{2+} diets, the nZnO diets inhibited the development of skeletal muscle cells and caused developmental damage (Fig. 3c). There was no significant change in the development of skeletal muscle between the nZnO (150 μg Zn per g diet) and the control group, indicating that the nZnO (150 μg Zn per g diet) met the early development of skeletal muscle cells (Fig. 3a and c). In contrast, the Zn^{2+} (150 μg Zn per g diet) significantly reduced the development of skeletal muscle cell area and led to an increase in intercellular space (Fig. 3a and c).

For the spinal cord, cell density was quantified as the ratio of cell area to unit spinal cord area (Fig. 3b). Although there was a trend of increasing spinal cord densities exposed to both Zn^{2+} (70 μg Zn per g diet) and nZnO (70 μg Zn per g diet) throughout developmental stages, both nZnO (70 μg Zn per g diet) were significantly lower than Zn^{2+} (70 μg Zn per g diet) at the same time point (Fig. 3d). For medaka exposed to

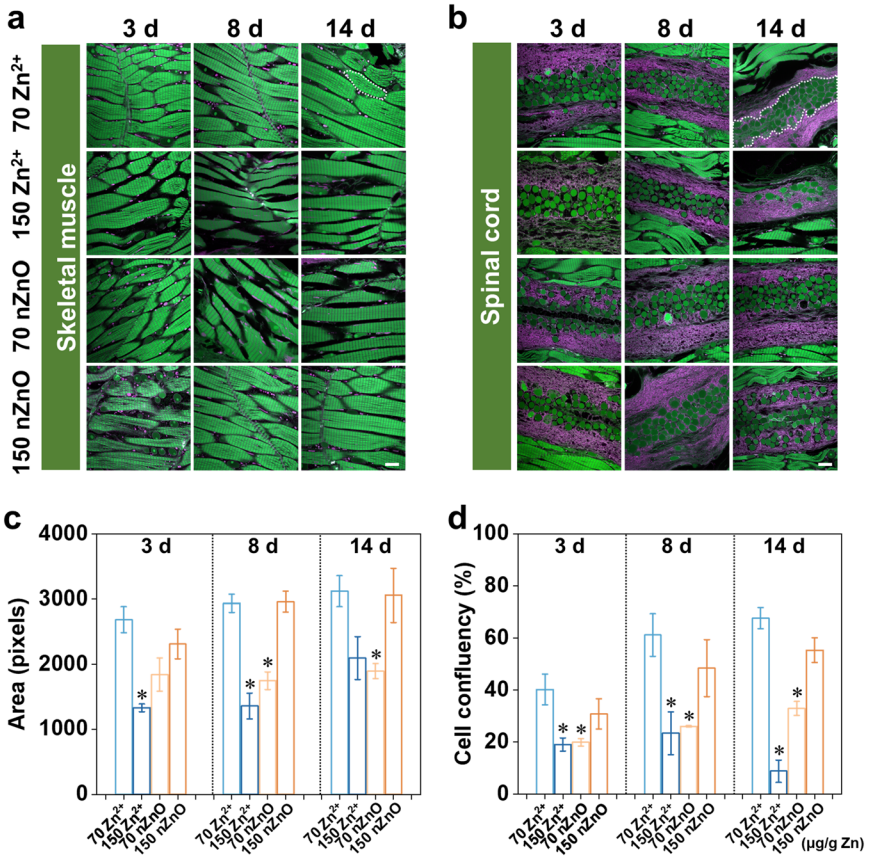

Fig. 3 Variation in expansion microscopy imaging and cellular quantification of medaka skeleton muscle system due to different Zn exposure. (a) Expansion microscopy imaging of skeleton muscle cells of medaka exposed to nZnO diets and Zn^{2+} diets during 14 d continuous exposure. (b) Expansion microscopy imaging of the spinal cord of medaka exposed to nZnO diets and Zn^{2+} diets during 14 d continuous exposure. (c) Quantification of variation in skeleton muscle cell area in medaka exposed to nZnO diets and Zn^{2+} diets. (d) Quantification of variation in cell confluency of the spinal cord in medaka exposed to nZnO diets and Zn^{2+} diets. Green, Alexa Fluor 488 NHS ester; magenta, ATTO 647 N NHS ester. Data were expressed as mean ± SD (n = 10). *$p < 0.05$, compared with the control (Zn^{2+} (70 μg Zn per g diet)). Scale bars: 10 μm. All length scales are presented in pre-expansion dimensions. The numbers 70 and 150 on the graph are the Zn contents in μg g^{-1}.

nZnO (150 μg Zn per g diet), skeletal muscle cell and spinal cord development were not significantly different from that of the controls during 14 d exposure, a trend similar to that of retinal cell development. nZnO (70 μg Zn per g diet) caused developmental damage due to the lack of nutrition of skeletal muscle cells and spinal cord compared with Zn^{2+}, and high concentrations of nZnO could improve this situation. However, the Zn^{2+} (150 μg Zn per g diet) significantly reduced spinal cord density and caused spinal cord developmental toxicity (Fig. 3b and d).

Variations in developmental patterns of digestive system in fish

In the digestive system, we focused on the length of intestinal microvilli. In conventional imaging methods, it is very challenging to achieve high-resolution imaging of microvilli due to their fineness and vulnerability to breakage. Whole-ExM perfectly solves this difficulty and enables the quantification of microvilli lengths. Intestinal microvilli increase the inner surface area of the intestine, thereby enhancing the efficiency of nutrient absorption, such as glucose and amino acids, which helps maintain energy balance and nutrient supply in fish.[59] In addition, microvilli can capture and clear microorganisms, toxins, and other harmful substances in the intestine, serving a defensive role.[60] Generally, longer microvilli are more favorable for maintaining intestinal stability and health, thus changes in microvilli length can indicate toxic effects on fish.[61] As indicated by the arrows in Fig. 4b, we measured the length of microvilli in the intestines and used the average length of microvilli in each image as the microvilli length for each sample. Microvillus length tended to increase in both the Zn^{2+} (70 μg Zn per g diet) and nZnO (70 μg Zn per g diet) treatments during 14-day exposure, and there was no significant change in the nZnO diets relative to the ionic Zn diets at the same developmental stages (Fig. 4a and c). For intestine development, there may not be a significant difference in effect between Zn^{2+} diets and nZnO diets. Notably, compared with the control group, the length of intestinal microvilli treated with nZnO (150 μg Zn per g diet) and Zn^{2+} (150 μg Zn per g diet) began to decrease

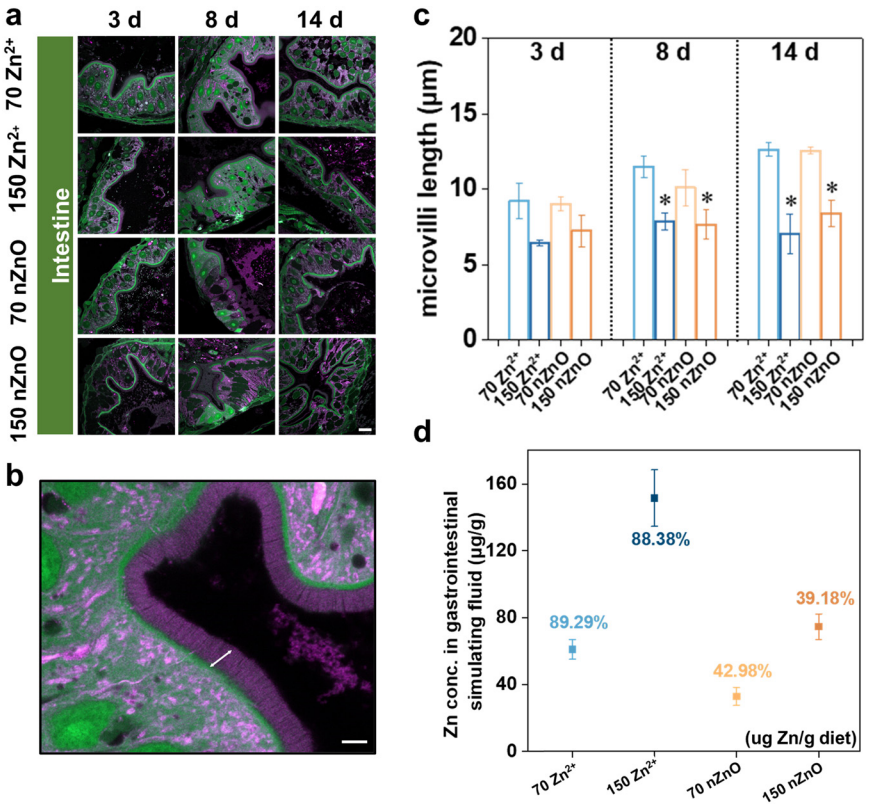

Fig. 4 Variation in expansion microscopy imaging and cellular quantification of medaka intestine due to different Zn exposure. (a) Expansion microscopy imaging of intestine microvilli of medaka exposed to nZnO diets and Zn^{2+} diets during 14 d continuous exposure. (b) Magnified view of a section of intestine, arrows indicated microvilli length measurement. (c) Quantification of variation in microvilli length medaka exposed to nZnO diets and Zn^{2+} diets. (d) *In vitro* dissolution rate of nZnO diets and Zn^{2+} diets after simulated gastrointestinal fluid test. The percentages on the graph represent the dissolution rate in gastrointestinal fluid. For (a) and (b), green, Alexa Fluor 488 NHS ester; magenta, ATTO 647 N NHS ester. Data were expressed as mean ± SD (n = 10). *$p < 0.05$, compared with the control (Zn^{2+} (70 μg Zn per g diet)). Scale bars: 10 μm. All length scales are presented in pre-expansion dimensions. The numbers 70 and 150 on the graph are the Zn content in μg g^{-1}.

significantly on days 3, 8, and 14, especially on day 14, Zn^{2+} (150 μg Zn per g diet) had a more obvious effect on the length of microvilli (Fig. 4a and c).

The results in the digestive system differed from those in the visual and skeletal muscle systems. When Zn from diets entered the gut, it bound to mucus in the intestinal epithelium and was subsequently translocated to epithelial cells as Zn^{2+} or bound to amino acids.[62] nZnO needs to be solubilized and absorbed in the gastrointestinal tract before it can enter the circulation to affect the retina and skeletal muscle, thus nZnO (70 μg Zn per g diet) may not be sufficient for the eye and skeletal muscle development. For the digestive system, the direct release of Zn^{2+} from nZnO in the gut made it very sensitive to elevated Zn levels, thus the nZnO (70 μg Zn per g diet) would meet the Zn requirements for gut development, whereas the nZnO (150 μg Zn per g diet) and Zn^{2+} (150 μg Zn per g diet) would be excessive for the gut and resulted in toxicity. It has been demonstrated that the addition of a 60 μg g^{-1} nZnO diet promotes probiotic colonization of the fish intestine.[62] In addition, the 60 μg g^{-1} nZnO diets upregulated genes associated with intestinal mucus secretion and promote the renewal of thrush cells in the intestinal villi. These probiotics share biological functions that ensure normal digestion, metabolism, nutrient supply, detoxification, promotion of intestinal motility, and immune and nutritional support for the gut.[36] Conversely, nZnO (70 μg Zn per g diet) down-regulate occludin and mucin gene expression in the fish intestine, along with reduced villus height, villus area, and goblet cell numbers, leading to impaired digestion, absorption, and immune functions.[63] This may be attributed to multiple factors. The accumulation of nZnO within cells could induce oxidative stress, thereby activating a series of cellular signaling pathways, such as the Nrf2/ARE pathway, which in turn regulates the expression of antioxidant genes. The activation of these signaling pathways can influence the physiological state of cells, subsequently affecting the development of microvilli.[64] In addition, nZnO can alter the composition of the gut microbiota, increasing the abundance of beneficial bacteria, such as Lactobacillus. These beneficial bacteria can produce short-chain fatty acids (SCFAs), which activate cellular signaling pathways *via* receptors like GPR41 and GPR43, promoting the proliferation of intestinal epithelial cells and the development of microvilli.[36] Overall, nZnO (70 μg Zn per g diet) promoted the normal development of intestinal villi and satisfied the intestinal Zn requirements,

whereas nZnO (150 μg Zn per g diet) was toxic to intestinal villi development.

We observed that in the visual and skeletal muscle systems, the low-level nZnO diet and high-level Zn^{2+} diet significantly inhibited cell growth and development, with no significant effect of the high-level nZnO diet. However, in the digestive system, this trend was reversed for nZnO, with a high-level nZnO diet and a high-level Zn^{2+} diet significantly inhibiting intestinal microvilli development, while low-level nZnO diet had no significant effect on microvilli

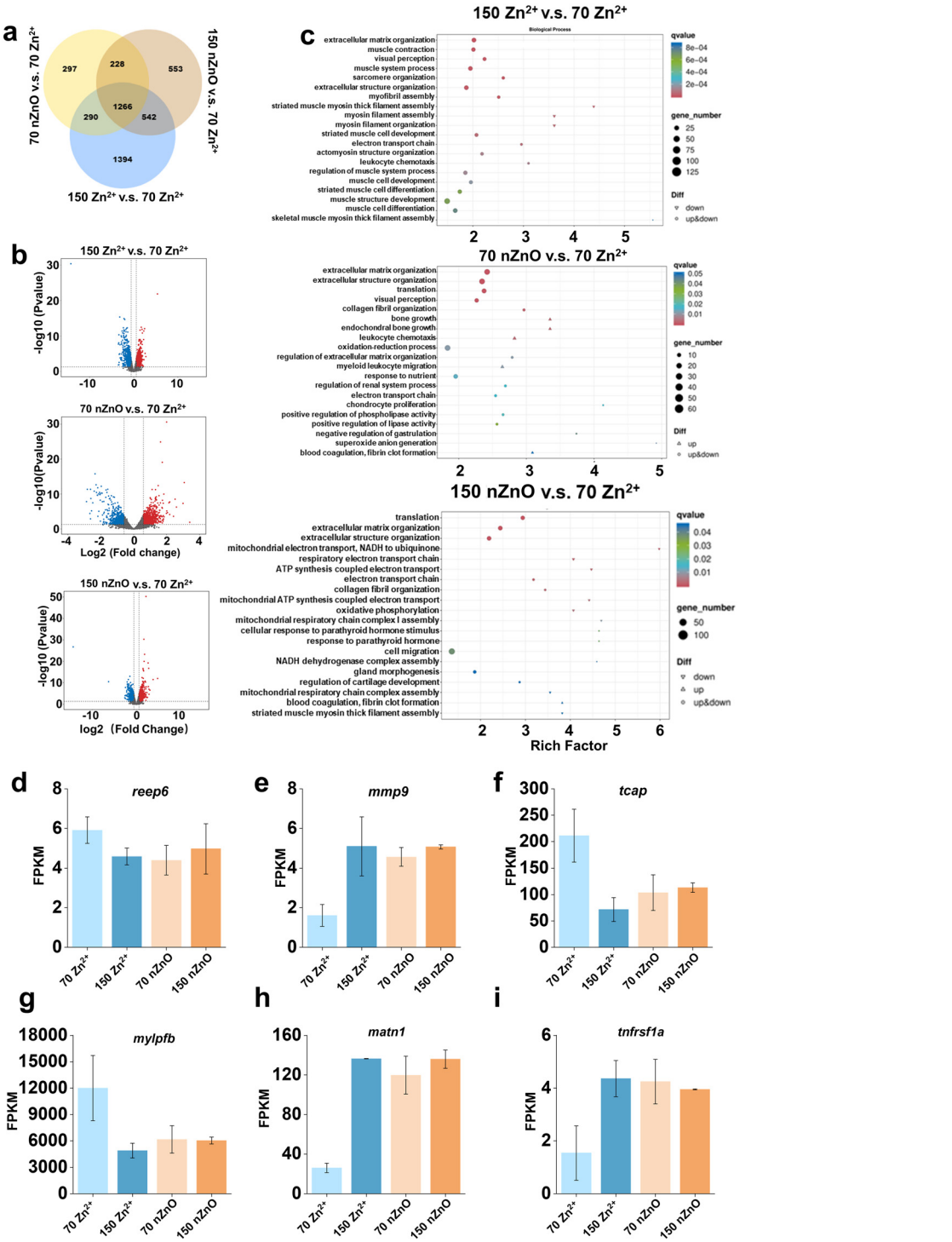

Fig. 5 RNA-sequencing results after treatment with nZnO diets and Zn^{2+} diets exposure. (a) Venn diagram of gene number in medaka transcriptome sequencing. (b) Differentially expressed genes analysis of medaka transcriptome results. (c) GO analysis of medaka transcriptome after nZnO diets and Zn^{2+} diets exposure. (d–f) Expression of differential genes associated with retinal development. (g–i) Expression of differential genes associated with skeleton muscle system development. The numbers 70 and 150 on the graph are the Zn content in μg g^{-1}.

development. To explore this phenomenon, we conducted *in vitro* simulated gastrointestinal fluid digestion tests to verify this phenomenon. Food digestion time in medaka gastrointestinal tracts ranged from 4–7 h.[65] In this test, the digestion time of diets in the simulated gastrointestinal fluid was set to 6 h to simulate the dissolution of Zn in the gastrointestinal tract of medaka.

The *in vitro* dissolution rate of nZnO diets was significantly lower than that of Zn^{2+} diets, possibly due to the tendency of nZnO to form aggregates, reducing Zn^{2+} release. Specifically, the Zn^{2+} (70 μg Zn per g diet) had an *in vitro* dissolution rate of 89.3% in simulated gastrointestinal fluid, producing ~62.5 μg g^{-1} Zn^{2+} in the gut. In contrast, nZnO (70 μg Zn per g diet) had an *in vitro* dissolution rate of only 43.0%, producing ~30 μg g^{-1} Zn^{2+}, which may be insufficient for retinal and skeletal muscle development. Conversely, nZnO (150 μg Zn per g diet) had an *in vitro* dissolution rate of 39.2%, releasing ~59 μg g^{-1} Zn^{2+}, which could meet the Zn requirements for retinal and skeletal muscle development, while the *in vitro* dissolution rate of Zn^{2+} (150 μg Zn per g diet) in simulated gastrointestinal fluid was 88.4%, producing up to 132.6 μg g^{-1} Zn^{2+}, which was toxic to the development of retina and skeletal muscle (Fig. 4d). These results also indirectly implied that the source of toxicity caused by ZnO *in vivo* was likely caused by Zn^{2+} dissolved in the body. Optimizing the physical and chemical properties of nZnO to enhance its dissolution rate in the gastrointestinal fluid and increase Zn^{2+} release was essential for improving its bioavailability and meeting the body's needs. Adjustment of parameters such as surface properties, particle size, and morphology of nZnO can effectively control its release, ensuring that sufficient Zn^{2+} is released at the appropriate time and location to meet the nutrient requirements of specific tissues such as the retina and skeletal muscle.

Transcriptomics of fish exposed to nZnO diets and Zn^{2+} diets

The above quantitative analysis of the imaging of different organs visualized the variation between the nZnO diets and the Zn^{2+} diets on the organ development of medaka. We confirmed the imaging results and analyzed the reasons by analyzing differential gene expression. We performed transcriptomic analysis of medaka exposed to Zn^{2+} (70 μg Zn per g diet), Zn^{2+} (150 μg Zn per g diet), nZnO (70 μg Zn per g diet), and nZnO (150 μg Zn per g diet) to illuminate the causes for the differences in toxicity. Using the reference genome of medaka, we analyzed transcriptomic data to investigate the content and expression patterns of genes associated with the visual system, skeletal muscle system, and digestive system. After 14 d exposure, compared to the control group, Venn diagram showed that 297, 553, and 1394 specific unigenes were expressed following exposure to nZnO (70 μg Zn per g diet), nZnO (150 μg Zn per g diet) and Zn^{2+} (70 μg Zn per g diet), respectively (Fig. 5a). In terms of differential gene expression, compared to the Zn^{2+} (70 μg Zn per g diet), the Zn^{2+} (150 μg Zn per g diet) led to differential expression of 3492 genes, with 1768 up-regulated and 1724 down-regulated genes (Fig. 5b). nZnO (70 μg Zn per g diet) treatment had 2081 differentially expressed genes, of which 994 were up-regulated and 1087 were down-regulated (Fig. 5b). nZnO (150 μg Zn per g diet) led to differential expression of 2589 genes, with 1429 up-regulated and 1160 down-regulated genes (Fig. 5b). GO analyses were performed and showed that for the Zn^{2+} (150 μg Zn per g diet) group, functions of differential genes were enriched in muscle contraction, visual perception, muscle system process, and sarcomere organization (Fig. 5c). For the nZnO (70 μg Zn per g diet), the differential genes were functionally enriched for functions related to visual perception, and skeletal growth (Fig. 5c). For the nZnO (150 μg Zn per g diet), there was no differential gene function enrichment in retinal and skeletal muscle development compared to the control group (Fig. 5c). These results were consistent with the above imaging results. Compared with the control, nZnO (150 μg Zn per g diet) exposure did not lead to significant differences in differential gene enrichment. In the imaging quantification results of the visual and skeletal muscle system, the nZnO (150 μg Zn per g diet) group and the Zn^{2+} (70 μg Zn per g diet) group had normal cell growth and development. nZnO (70 μg Zn per g diet) and Zn^{2+} (150 μg Zn per g diet) showed significant differential gene enrichment during the development of the visual and skeletal muscle systems. Combined with the imaging results, the nZnO (70 μg Zn per g diet) may not meet the early developmental needs, resulting in significant differential enrichment of differential genes related to vision and skeletal muscle. The Zn^{2+} (150 μg Zn per g diet) provided excessive Zn levels, resulting in significant differential enrichment of differential genes related to vision and skeletal muscle, which in turn caused cell toxicity.

We then selected the genes related to organ development and compared the gene expression levels between Zn^{2+} (150 μg Zn per g diet), nZnO (70 μg Zn per g diet), nZnO (150 μg Zn per g diet), and Zn^{2+} (70 μg Zn per g diet) for comparative analysis by FPKM values. For the retina, we screened two genes related to retinal development, *reep6* and *mmp9*. Compared to the Zn^{2+} (70 μg Zn per g diet), down-regulation and up-regulation of *reep6* and *mmp9* genes, respectively, were observed in medaka exposed to Zn^{2+} (150 μg Zn per g diet) and two nZnO diets (Fig. 5d and e). It was reported that knockout of *reep6* in mice and zebrafish results in retinal cell death, and *reep6* serves as a critical target for NRL in maintaining the photoreceptor function and homeostasis of rod cells which mediated black-and-white vision and peripheral vision.[66] Following damage to photoreceptors, Müller glial cells and photoreceptor progenitor cells derived from Müller glia induced the expression of *mmp-9*.[67] For the skeletal muscle system, the results showed that the expression of different genes involved the *tcap*, *mylpfb*, *matn1*, and *tnfrsf1a* genes (Fig. 5f–i). Compared to the control, medaka exposed to the other three diets showed downregulation of the *tcap* and *mylpfb* genes, respectively, and the *matn1* and *tnfrsf1a* genes showed upregulation,

respectively (Fig. 5f–i). It has been found that a reduction in *tcap* lead to a myotonic dystrophy-like phenotype, including deformation of muscle structure and impaired swimming ability.[68] It was observed that *tcap* in zebrafish, which may play a role in stretch sensor signaling, displays a fluctuating expression pattern throughout somitogenesis. Notably, this variable expression can be triggered by the application of stretch force. Furthermore, the expression level of *tcap* is under negative regulation by integrin-link kinase (ILK), a key protein kinase implicated in the stretch sensing signaling pathway. These findings have led to the proposal of an intriguing new hypothesis. It posits that the transcription level of *tcap* is modulated by stretch force, thereby ensuring the proper interaction between sarcomeres and the muscle membrane in striated muscles.[68] The gene *mylpfb* encodes myosin light chains, which are structural proteins in muscle that are involved in the movement of muscle fibers during muscle contraction.[69] A study has found that mutations in the *mylpfb* can lead to a new type of segmental muscular dysplasia, manifested as distal joint contracture. The *mylpfb* encodes a fast skeletal muscle regulating light chain, and its mutation in a mouse model results in complete absence of skeletal muscle at birth and rapid death from respiratory failure, indicating that this gene plays an important role in muscle development and contraction.[70] The gene *matn1* encodes a protein in skeletal muscle which played an important role in the structure and function of skeletal muscle, and its mutation or aberrant expression may lead to abnormal development or dysfunction of skeletal muscle.[71] Additionally, the *tnfrsf1a* gene is important in the growth and development of bone marrow stem cells.[72] A research has found that TNF α has different regulatory effects on the behavior of hematopoietic stem cells (HSCs) and the function of bone marrow stromal cells through its receptors TNFRSF1A and TNFRSF1B. The deficiency of TNFRSF1A can lead to impaired repair of bone marrow stromal cells, affecting the effectiveness of hematopoietic stem cell transplantation.[73] We hypothesized that cell development was affected by gene expression at the transcriptional level.[74] The accumulation of nZnO within cells may lead to oxidative stress, activating the Nrf2/ARE pathway and regulating the expression of antioxidant genes. Additionally, nZnO may trigger inflammatory responses, activating inflammatory signaling pathways such as NF-κB, leading to the release of cytokines like IL-1β and TNF-α. Excessive intake of Zn^{2+} may cause cytotoxicity, especially when its concentration exceeds the cell's tolerance limit. Zn^{2+} can affect cell proliferation and differentiation, leading to apoptosis, which in turn impacts the development of organs.[75] Therefore, the variation in effects on medaka organs caused by nZnO diets and Zn^{2+} diets may be due to the different expressions of several specific genes.

In the cellular processes-related pathways, genes within the categories of "focal adhesion" and "regulation of actin cytoskeleton" were significantly altered in both low nZnO (70 μg Zn per g diet) *vs.* Zn^{2+} (70 μg Zn per g diet), high nZnO

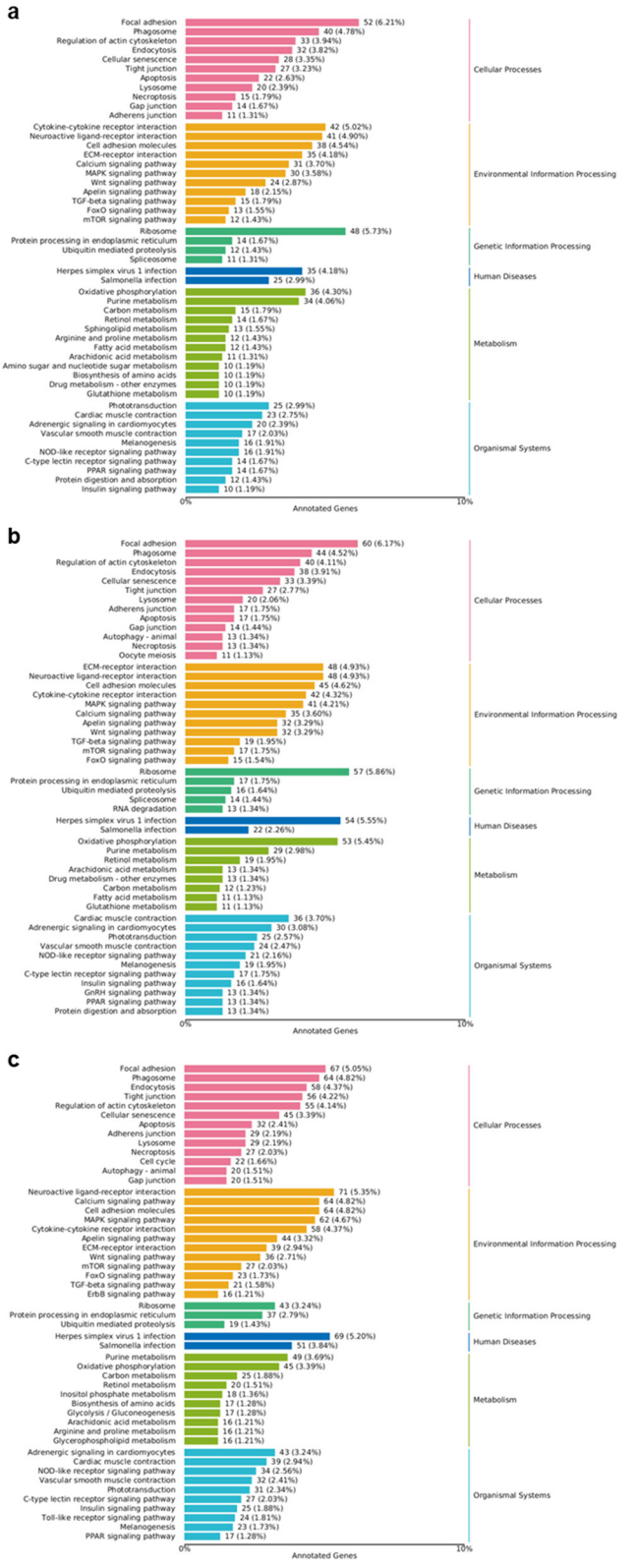

Fig. 6 RNA-sequencing results after treatment with nZnO diets and Zn^{2+} diets exposure. (a) KEGG pathway annotation for nZnO (70 μg Zn per g diet) *vs.* Zn^{2+} (70 μg Zn per g diet). (b) KEGG pathway annotation for nZnO (150 μg Zn per g diet) *vs.* Zn^{2+} (70 μg Zn per g diet). (c) KEGG pathway annotation for Zn^{2+} (150 μg Zn per g diet) *vs.* Zn^{2+} (70 μg Zn per g diet).

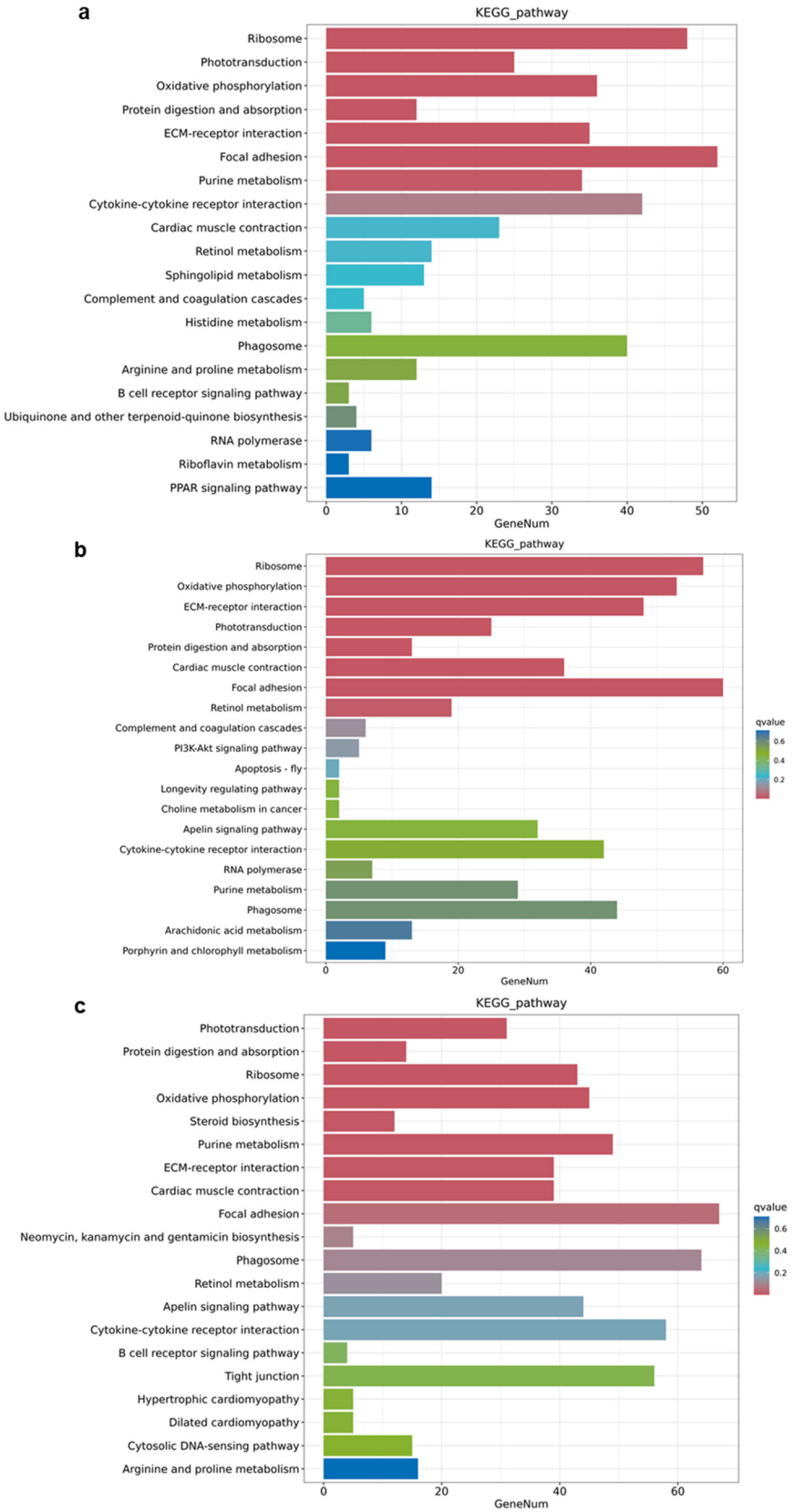

Fig. 7 RNA-sequencing results after treatment with nZnO diets and Zn^{2+} diets exposure. (a) KEGG pathway enrichment analysis for nZnO (70 μg Zn per g diet) *vs.* Zn^{2+} (70 μg Zn per g diet). (b) KEGG pathway enrichment analysis for nZnO (150 μg Zn per g diet) *vs.* Zn^{2+} (70 μg Zn per g diet). (c) KEGG pathway enrichment analysis for Zn^{2+} (150 μg Zn per g diet) *vs.* Zn^{2+} (70 μg Zn per g diet).

(150 μg Zn per g diet) *vs.* Zn^{2+} (70 μg Zn per g diet) treatments and high Zn^{2+} (150 μg Zn per g diet) *vs.* Zn^{2+} (70 μg Zn per g diet) treatments (Fig. 6a–c). Thus, different concentrations and forms of Zn may affect the regulation of cell adhesion and cytoskeleton, which in turn affect cell migration, morphology, and other functions.[76] The genes related to MAPK signaling pathway, calcium signaling pathway, apelin signaling pathway, and Wnt signaling pathway were affected in both treatments. Among them, calcium signaling pathway plays an important role in the development of eyes, muscles, and intestines.[77] Wnt signaling pathway regulates cell polarity and cell migration, which plays an important role in the development of muscles and intestines.[78] The differential expression of genes in these pathways was more obvious in the high-level nZnO diet than in the low-level nZnO diet (Fig. 6a and b). This suggested that the high-level nZnO may cause greater disruption to these key signaling pathways, resulting in more severe cellular functional imbalances.[79] In the metabolism-related pathways, genes associated with purine metabolism and retinol metabolism changed in both treatments. Under high-level nZnO diet treatment, the differential expression of genes in these metabolic pathways was more significant (Fig. 6a and b). This implied that high level nZnO may have a greater impact on cellular energy metabolism and lipid metabolism, leading to more serious nutritional imbalance.[80] Notably, a high-level Zn^{2+} diet exhibited higher differential gene expression in these pathways, likely due to the dissolution of Zn^{2+} *in vivo* (Fig. 6c). In addition, we compared the impacts of the two nZnO treatments and high-level Zn^{2+} diet on medaka by KEGG pathway enrichment analysis of differentially expressed genes. Both low and high-level nZnO diets and high-level Zn^{2+} diet significantly affected some key biological pathways and processes (Fig. 7a–c). Among them, the pathways of ribosome, oxidative phosphorylation, and ECM–receptor interaction were affected at both concentrations, suggesting that nZnO may interfere with protein synthesis, energy metabolism, cell migration, and tissue localization in medaka (Fig. 7a and b). This suggested that ZnO nanoparticles may induce toxicity by interfering with cellular protein synthesis, energy metabolism, and cell migration and organization.[81] It is worth noting that low-level nZnO were more sensitive to affect nutrient metabolism and organ function, while high-level nZnO were more likely to cause imbalance in cell structure and function.

Conclusions

We employed novel expansion microscopy (ExM) to achieve, for the first time, nanoscale resolution imaging of the toxic effects of nanomaterials on early organ development in fish, specifically assessing the toxicity of nZnO. ExM enabled the direct quantification of toxic effects on cells at different developmental stages with nanoscale resolution, overcoming the limitations of traditional tissue section staining methods, which may introduce artifacts during sample preparation and have restricted observation resolution that complicates accurate detection of nanoscale structural changes. We conducted a comprehensive evaluation of the toxic effects of nZnO and Zn^{2+} on the visual, skeletal muscle, and digestive systems, as well as the sources of nZnO toxicity. Our findings indicated that nZnO concentrations suitable for the development of the visual and skeletal muscle systems may lead to potential excessive toxicity in the digestive system. Conversely, concentrations appropriate for digestive system development may be insufficient for the needs of the visual and skeletal muscle systems. This difference in toxicity probably resulted from the different solubility and bioavailability of nZnO in gastrointestinal fluids. Further RNA sequencing results revealed differential sensitivity of various organs to nanomaterial exposure, underscoring the necessity for comprehensive risk assessment strategies in toxicology. This study provided theoretical support for the safe application of nanomaterials in the biomedical field through the evaluation of their toxic effects *via* ExM.

Data availability

The resequencing raw data of medaka (*Oryzias melastigma*, wild type) in this study have been uploaded to the NCBI Sequence Reading Archive (SRA) with accession number PRJNA1141718. **https://www.ncbi.nlm.nih.gov/sra/?term=PRJNA1141718**.

Conflicts of interest

There are no conflicts to declare.

Acknowledgements

We thank the anonymous reviewers for their helpful comments. Our study was supported by the Shenzhen Municipal Science and Technology Innovation Commission (JCYJ20210324134000001), and Hong Kong Research Grants Council (CityU 11102321).

References

1 M. E. Vance, T. Kuiken, E. P. Vejerano, S. P. McGinnis, M. F. Hochella Jr, D. Rejeski and M. S. Hull, Nanotechnology in the real world: Redeveloping the nanomaterial consumer products inventory, *Beilstein J. Nanotechnol.*, 2015, **6**(1), 1769–1780.
2 S. Mitragotri, D. G. Anderson, X. Chen, E. K. Chow, D. Ho, A. V. Kabanov, J. M. Karp, K. Kataoka, C. A. Mirkin and S. H. Petrosko, *et al.*, Accelerating the Translation of Nanomaterials in Biomedicine, *ACS Nano*, 2015, **9**(7), 6644–6654.
3 Y. Cohen, R. Rallo, R. Liu and H. H. Liu, In Silico Analysis of Nanomaterials Hazard and Risk, *Acc. Chem. Res.*, 2013, **46**(3), 802–812.
4 T. Buerki-Thurnherr, K. Schaepper, L. Aengenheister and P. Wick, Developmental Toxicity of Nanomaterials: Need for a

Better Understanding of Indirect Effects, *Chem. Res. Toxicol.*, 2018, **31**(8), 641–642.
5 Z. Y. Chen, Y. C. Yang, B. J. Wang, F. Y. Cheng, Y. L. Lee, Y. H. Lee and Y. J. Wang, Comparing different surface modifications of zinc oxide nanoparticles in the developmental toxicity of zebrafish embryos and larvae, *Ecotoxicol. Environ. Saf.*, 2022, **243**, 113967.
6 M. Tsoli, H. Kuhn, W. Brandau, H. Esche and G. Schmid, Cellular uptake and toxicity of Au55 clusters, *Small*, 2005, **1**(8–9), 841–844.
7 O. Kose, P. Mantecca, A. Costa and M. Carrière, Putative adverse outcome pathways for silver nanoparticle toxicity on mammalian male reproductive system: a literature review, *Part. Fibre Toxicol.*, 2023, **20**(1), 1.
8 P. Ganguly, A. Breen and S. C. Pillai, Toxicity of nanomaterials: exposure, pathways, assessment, and recent advances, *ACS Biomater. Sci. Eng.*, 2018, **4**(7), 2237–2275.
9 M. Ajdary, M. A. Moosavi, M. Rahmati, M. Falahati, M. Mahboubi, A. Mandegary, S. Jangjoo, R. Mohammadinejad and R. S. Varma, Health concerns of various nanoparticles: A review of their *in vitro* and *in vivo* toxicity, *Nanomaterials*, 2018, **8**(9), 634–662.
10 M. Srinivasan, D. Sedmak and S. Jewell, Effect of fixatives and tissue processing on the content and integrity of nucleic acids, *Am. J. Pathol.*, 2002, **161**(6), 1961–1971.
11 K. B. Tierney, Behavioural assessments of neurotoxic effects and neurodegeneration in zebrafish, *Biochim. Biophys. Acta, Mol. Basis Dis.*, 2011, **1812**(3), 381–389.
12 J. Lee, D. Y. Hyeon and D. Hwang, Single-cell multiomics: technologies and data analysis methods, *Exp. Mol. Med.*, 2020, **52**(9), 1428–1442.
13 Y. H. Mir, A. Qin, S. Mir, S. U. Rahman, M. Mushtaq, M. A. Ganie, M. Chesti, J. A. Bhat, Z. A. Baba and M. A. Bhat, Nano-Scale Secondary Ion Mass Spectrometry: A Paradigm Shift in Soil Science, *J. Spectrosc.*, 2024, **2024**(1), 3625623.
14 T. Ozawa, H. Yoshimura and S. B. Kim, Advances in fluorescence and bioluminescence imaging, *Anal. Chem.*, 2013, **85**(2), 590–609.
15 N. I. Zheludev and G. Yuan, Optical superoscillation technologies beyond the diffraction limit, *Nat. Rev. Phys.*, 2022, **4**(1), 16–32.
16 M. Gao, Expansion microscopy opens the door to exploring more challenges, *Nat. Methods*, 2022, **19**(2), 147–148.
17 M. G. Gustafsson, Surpassing the lateral resolution limit by a factor of two using structured illumination microscopy, *J. Microsc.*, 2000, **198**(2), 82–87.
18 S. W. Hell, Far-Field Optical Nanoscopy, *Science*, 2007, **316**(5828), 1153–1158.
19 M. J. Ust, M. Bates and X. Zhuang, Sub-diffraction-limit imaging by stochastic optical reconstruction microscopy (STORM), *Nat. Methods*, 2006, **3**(10), 793–796.
20 B. R. Gallagher and Y. Zhao, Expansion microscopy: A powerful nanoscale imaging tool for neuroscientists, *Neurobiol. Dis.*, 2021, **154**, 105362.
21 A. T. Wassie, Y. Zhao and E. S. Boyden, Expansion microscopy: principles and uses in biological research, *Nat. Methods*, 2019, **16**(1), 33–41.
22 A. Klimas and Y. Zhao, Expansion microscopy: toward nanoscale imaging of a diverse range of biomolecules, *ACS Nano*, 2020, **14**(7), 7689–7695.
23 G. Wen, V. Leen, T. Rohand, M. Sauer and J. Hofkens, Current progress in expansion microscopy: chemical strategies and applications, *Chem. Rev.*, 2023, **123**(6), 3299–3323.
24 B. A. Wilt, L. D. Burns, E. T. Wei Ho, K. K. Ghosh, E. A. Mukamel and M. J. Schnitzer, Advances in light microscopy for neuroscience, *Annu. Rev. Neurosci.*, 2009, **32**, 435–506.
25 A. Acke, S. Van Belle, B. Louis, R. Vitale, S. Rocha, T. Voet, Z. Debyser and J. Hofkens, Expansion microscopy allows high resolution single cell analysis of epigenetic readers, *Nucleic Acids Res.*, 2022, **50**(17), 100.
26 M. Connolly, M. Fernández, E. Conde, F. Torrent, J. M. Navas and M. L. Fernández-Cruz, Tissue distribution of zinc and subtle oxidative stress effects after dietary administration of ZnO nanoparticles to rainbow trout, *Sci. Total Environ.*, 2016, **551**, 334–343.
27 J. Jiang, J. Pi and J. Cai, The advancing of zinc oxide nanoparticles for biomedical applications, *Bioinorg. Chem. Appl.*, 2018, **2018**(1), 1062562.
28 M. Ghosh, S. Sinha, M. Jothiramajayam, A. Jana, A. Nag and A. Mukherjee, Cyto-genotoxicity and oxidative stress induced by zinc oxide nanoparticle in human lymphocyte cells in vitro and Swiss albino male mice *in vivo*, *Food Chem. Toxicol.*, 2016, **97**, 286–296.
29 E. R. Bordin, W. A. Ramsdorf, L. M. L. Domingos, L. P. de Souza Miranda, N. P. Mattoso Filho and M. M. Cestari, Ecotoxicological effects of zinc oxide nanoparticles (ZnO-NPs) on aquatic organisms: Current research and emerging trends, *J. Environ. Manage.*, 2024, **349**, 119396.
30 A. Sun, B. Z. Tang, K. W.-K. Tsim and W.-X. Wang, Unique interplay between Zn 2+ and nZnO determined the dynamic cellular stress in zebrafish cells, *Environ. Sci.: Nano*, 2021, **8**(8), 2324–2335.
31 I. Blinova, A. Ivask, M. Heinlaan, M. Mortimer and A. Kahru, Ecotoxicity of nanoparticles of CuO and ZnO in natural water, *Environ. Pollut.*, 2010, **158**(1), 41–47.
32 D. Fernández, C. García-Gómez and M. Babín, *In vitro* evaluation of cellular responses induced by ZnO nanoparticles, zinc ions and bulk ZnO in fish cells, *Sci. Total Environ.*, 2013, **452**, 262–274.
33 V. Sloup, I. Jankovská, S. Nechybová, P. Peřinková and I. Langrová, Zinc in the animal organism: a review, *Scientia Agriculturae Bohemica*, 2017, **48**(1), 13–21.
34 K. J. Ong, X. Zhao, M. E. Thistle, T. J. MacCormack, R. J. Clark, G. Ma, Y. Martinez-Rubi, B. Simard, J. S. C. Loo and J. G. Veinot, Mechanistic insights into the effect of nanoparticles on zebrafish hatch, *Nanotoxicology*, 2014, **8**(3), 295–304.
35 B. Wang, W. Feng, M. Wang, T. Wang, Y. Gu, M. Zhu, H. Ouyang, J. Shi, F. Zhang and Y. Zhao, Acute toxicological

impact of nano-and submicro-scaled zinc oxide powder on healthy adult mice, *J. Nanopart. Res.*, 2008, **10**, 263–276.

36 S. Ma and W.-X. Wang, Reshaping fish intestinal microbiota and facilitating barrier function by ZnO nanoparticles, *Environ. Sci.: Nano*, 2023, **10**(9), 2259–2272.

37 J. Sim, C. E. Park, I. Cho, K. Min, M. Eom, S. Han, H. Jeon, H.-J. Cho, E.-S. Cho and A. Kumar, Nanoscale resolution imaging of the whole mouse embryos and larval zebrafish using expansion microscopy, *BioRxiv*, 2021, preprint, DOI: **10.1101/2021.05.18.443629**.

38 M. Minekus, M. Alminger, P. Alvito, S. Ballance, T. Bohn, C. Bourlieu, F. Carrière, R. Boutrou, M. Corredig and D. Dupont, A standardised static in vitro digestion method suitable for food–an international consensus, *Food Funct.*, 2014, **5**(6), 1113–1124.

39 M. Wang and W.-X. Wang, Meeting Zn needs during medaka eye development: Nanoscale visualization of retina by expansion microscopy, *Environ. Sci. Technol.*, 2022, **56**(22), 15780–15790.

40 Z. Chen, X. Zhu, X. Lv, Y. Huang, W. Qian, P. Wang, B. Li, Z. Wang and Z. Cai, Alleviative Effects of C(60) on the Trophic Transfer of Cadmium along the Food Chain in Aquatic Environment, *Environ. Sci. Technol.*, 2019, **53**(14), 8381–8388.

41 F. Chen, P. W. Tillberg and E. S. Boyden, Expansion Microscopy, *Science*, 2015, **347**(6221), 543–548.

42 K. Derevtsova, E. Pchitskaya, A. Rakovskaya and I. Bezprozvanny, Applying the expansion microscopy method in neurobiology, *J. Evol. Biochem. Physiol.*, 2021, **57**(3), 681–693.

43 B. H. Grahn, P. G. Paterson, K. T. Gottschall-Pass and Z. Zhang, Zinc and the eye, *J. Am. Coll. Nutr.*, 2001, **20**(2), 106–118.

44 D. Zheng, G. P. Feeney, P. Kille and C. Hogstrand, Regulation of ZIP and ZnT zinc transporters in zebrafish gill: zinc repression of ZIP10 transcription by an intronic MRE cluster, *Physiol. Genomics*, 2008, **34**(2), 205–214.

45 M. V. Do Carmo e Sa, L. E. Pezzato, M. M. Barros and P. De Magalhaes Padilha, Relative bioavailability of zinc in supplemental inorganic and organic sources for Nile tilapia Oreochromis niloticus fingerlings, *Aquacult. Nutr.*, 2005, **11**(4), 273–281.

46 B. H. Grahn, P. G. Paterson, K. T. Gottschall-Pass and Z. Zhang, Zinc and the eye, *J. Am. Coll. Nutr.*, 2001, **20**(2), 106–118.

47 M. Ugarte and N. N. Osborne, Zinc in the retina, *Prog. Neurobiol.*, 2001, **64**(3), 219–249.

48 I. Papagiannis, I. Kagalou, J. Leonardos, D. Petridis and V. Kalfakakou, Copper and zinc in four freshwater fish species from Lake Pamvotis (Greece), *Environ. Int.*, 2004, **30**(3), 357–362.

49 R. Strack, Bigger is better for super-resolution, *Nat. Methods*, 2015, **12**(3), 169.

50 S. Truckenbrodt, C. Sommer, S. O. Rizzoli and J. G. Danzl, A practical guide to optimization in X10 expansion microscopy, *Nat. Protoc.*, 2019, **14**(3), 832–863.

51 K. Taslima, M. Al-Emran, M. S. Rahman, J. Hasan, Z. Ferdous, M. F. Rohani and M. Shahjahan, Impacts of heavy metals on early development, growth and reproduction of fish–A review, *Toxicol. Rep.*, 2022, **9**, 858–868.

52 F. De Busserolles, J. L. Fitzpatrick, N. J. Marshall and S. P. Collin, The influence of photoreceptor size and distribution on optical sensitivity in the eyes of lanternfishes (Myctophidae), *PLoS One*, 2014, **9**(6), 99957.

53 M. Hoon, H. Okawa, L. Della Santina and R. O. Wong, Functional architecture of the retina: development and disease, *Prog. Retinal Eye Res.*, 2014, **42**, 44–84.

54 D. G. SSfakianakis, E. Renieri, M. Kentouri and A. M. Tsatsakis, Effect of heavy metals on fish larvae deformities: A review, *Environ. Res.*, 2015, **137**, 246–255.

55 G. K. Zupanc, Adult neurogenesis in the central nervous system of teleost fish: from stem cells to function and evolution, *J. Exp. Biol.*, 2021, **224**(8), 226–357.

56 A. Rowlerson, Cellular mechanisms of post-embryonic muscle growth in aquaculture species. In: Johnston IA (ed) Muscle Development and Growth, *Fish Physiol.*, 2001, **18**, 103–140.

57 L. C. Rome, D. Swank and D. Corda, How fish power swimming, *Science*, 1993, **261**(5119), 340–343.

58 E. Miramontes, P. Mozdziak, J. N. Petitte, M. Kulus, M. Wieczorkiewicz and B. Kempisty, Skeletal muscle and the effects of ammonia toxicity in fish, mammalian, and avian species: A comparative review based on molecular research, *Int. J. Mol. Sci.*, 2020, **21**(13), 4641.

59 P. R. Kiela and F. K. Ghishan, Physiology of Intestinal Absorption and Secretion, *Best Pract. Res., Clin. Gastroenterol.*, 2016, **30**(2), 145–159.

60 M. B. Rust, Nutritional physiology, *Fish Nutr.*, 2003, 367–452.

61 E. RRingø, Z. Zhou, J. G. Vecino, S. Wadsworth, J. Romero, Å. Krogdahl, R. E. Olsen, A. Dimitroglou, A. Foey and S. Davies, Effect of dietary components on the gut microbiota of aquatic animals. A never-ending story?, *Aquacult. Nutr.*, 2016, **22**(2), 219–282.

62 C. Hogstrand, P. Kille, R. I. Nicholson and K. M. Taylor, Zinc transporters and cancer: a potential role for ZIP7 as a hub for tyrosine kinase activation, *Trends Mol. Med.*, 2009, **15**(3), 101–111.

63 G. Santos, M. C. Miguel Libanori, S. Pereira Dutra, J. V. S. Ferrarezi, M. B. Ferreira, T. A. Soligo, E. Yamashita, M. Martins and J. L. Mouriño, Probiotic mix of Bacillus spp. and benzoic organic acid as growth promoter against Streptococcus agalactiae in *Nile tilapia*, *Aquaculture*, 2022, **566**, 739212.

64 A. Sun, S. Ma and W. X. Wang, Two-sided cellular and physiological effects of zinc oxide nanoparticles (nZnO): a critical review, *Environ. Sci.: Nano*, 2024, DOI: **10.1039/D4EN00676C**.

65 A. Uscanga, F. J. Moyano and C. A. Alvarez, Assessment of enzymatic efficiency on protein digestion in the tilapia Oreochromis niloticus, *Fish Physiol. Biochem.*, 2010, **36**(4), 1079–1085.

66 H. Hao, S. Veleri, B. Sun, D. S. Kim, P. W. Keeley, J.-W. Kim, H.-J. Yang, S. P. Yadav, S. H. Manjunath and R. Sood, *et al.*, Regulation of a novel isoform of Receptor Expression Enhancing Protein REEP6 in rod photoreceptors by bZIP

transcription factor NRL, *Hum. Mol. Genet.*, 2014, **23**(16), 4260–4271.

67 N. J. Silva, M. Nagashima, J. Li, L. Kakuk-Atkins, M. Ashrafzadeh, D. R. Hyde and P. F. Hitchcock, Inflammation and matrix metalloproteinase 9 (Mmp-9) regulate photoreceptor regeneration in adult zebrafish, *Glia*, 2020, **68**(7), 1445–1465.

68 R. Zhang, J. Yang, J. Zhu and X. Xu, Depletion of zebrafish Tcap leads to muscular dystrophy via disrupting sarcomere–membrane interaction, not sarcomere assembly, *Hum. Mol. Genet.*, 2009, **18**(21), 4130–4140.

69 J. X. Chong, J. C. Talbot, E. M. Teets, S. Previs, B. L. Martin, K. M. Shively, C. T. Marvin, A. S. Aylsworth, R. Saadeh-Haddad and U. A. Schatz, Mutations in MYLPF cause a novel segmental amyoplasia that manifests as distal arthrogryposis, *Am. J. Hum. Genet.*, 2020, **107**(2), 293–310.

70 P. Kaewsatuan, C. Poompramun, S. Kubota, J. Yongsawatdigul, W. Molee, P. Uimari and A. Molee, Thigh muscle metabolic response is linked to feed efficiency and meat characteristics in slow-growing chicken, *Poult. Sci.*, 2023, **102**(7), 102741.

71 L. N. Luderman, G. Unlu and E. W. Knapik, Chapter Three - Zebrafish Developmental Models of Skeletal Diseases, *Curr. Top. Dev. Biol.*, 2017, **124**, 81–124.

72 (*a*) L. Cavone, T. McCann, L. K. Drake, E. A. Aguzzi, A.-M. Oprişoreanu, E. Pedersen, S. Sandi, J. Selvarajah, T. M. Tsarouchas and D. Wehner, A unique macrophage subpopulation signals directly to progenitor cells to promote regenerative neurogenesis in the zebrafish spinal cord, *Dev. Cell*, 2021, **56**(11), 1617–1630.

73 J. M. SanMiguel, E. Eudy, M. A. Loberg, K. A. Young, J. J. Mistry, K. D. Mujica, L. S. Schwartz, T. M. Stearns, G. A. Challen and J. J. Trowbridge, Distinct Tumor Necrosis Factor Alpha Receptors Dictate Stem Cell Fitness versus Lineage Output in Dnmt3a-Mutant Clonal Hematopoiesis, *Cancer Discovery*, 2022, **12**(12), 2763–2773.

74 J. Xiao and W.-X. Wang, Patterns and Crucial Regulation of Alternative Splicing During Early Development in Zebrafish, *J. Mol. Biol.*, 2022, **434**(21), 167821.

75 N. Levaot and M. Hershfinkel, How cellular Zn(2+) signaling drives physiological functions, *Cell Calcium*, 2018, **75**, 53–63.

76 X. Xu, Y. Tang, Y. Lang, Y. Liu, W. Cheng, H. Xu and Y. Liu, Oral Exposure to ZnO Nanoparticles Disrupt the Structure of Bone in Young Rats via the OPG/RANK/RANKL/IGF-1 Pathway, *Int. J. Nanomed.*, 2020, **15**, 9657–9668.

77 J. Xu, A. Zeug, B. Riederer, S. Yeruva, O. Griesbeck, H. Daniel, B. Tuo, E. Ponimaskin, H. Dong and U. Seidler, Calcium-sensing receptor regulates intestinal dipeptide absorption via Ca^{2+} signaling and IKCa activation, *Physiol. Rep.*, 2020, **8**(1), e14337.

78 J. Von Maltzahn, N. C. Chang, C. F. Bentzinger and M. A. Rudnicki, Wnt signaling in myogenesis, *Trends Cell Biol.*, 2012, **22**(11), 602–609.

79 L. Taccola, V. Raffa, C. Riggio, O. Vittorio, M. C. Iorio, R. Vanacore, A. Pietrabissa and A. Cuschieri, Zinc oxide nanoparticles as selective killers of proliferating cells, *Int. J. Nanomed.*, 2011, **6**, 1129–1140.

80 T. Xia, M. Kovochich, M. Liong, L. Mädler, B. Gilbert, H. Shi, J. I. Yeh, J. I. Zink and A. E. Nel, Comparison of the Mechanism of Toxicity of Zinc Oxide and Cerium Oxide Nanoparticles Based on Dissolution and Oxidative Stress Properties, *ACS Nano*, 2008, **2**(10), 2121–2134.

81 C. A. Dieni, N. I. Callaghan, P. T. Gormley, K. M. A. Butler and T. J. MacCormack, Physiological hepatic response to zinc oxide nanoparticle exposure in the white sucker, Catostomus commersonii, *Comp. Biochem. Physiol., Part C: Toxicol. Pharmacol.*, 2014, **162**, 51–61.

